

# Synthesis and properties of the theoretically predicted mixed-valent perovskite superconductors: $\text{CsTlX}_3$ (X = F, Cl)

M. Retuerto<sup>1</sup>, T. Emge<sup>1</sup>, M. R. Li<sup>1</sup>, Z. P. Yin<sup>2</sup>, M. Croft<sup>2</sup>, A. Ignatov<sup>2</sup>, P. W. Stephens<sup>3</sup>, J. Hadermann<sup>4</sup>, J. W. Simonson<sup>3</sup>, M. C. Aronson<sup>3,5</sup>, A. Pan<sup>6</sup>, D. N. Basov<sup>6</sup>, G. Kotliar<sup>2</sup>, M. Greenblatt<sup>1\*</sup>

<sup>1</sup> Department of Chemistry and Chemical Biology, Rutgers, The State University of New Jersey, 610 Taylor Road, Piscataway, NJ 08854, USA

<sup>2</sup> Department of Physics and Astronomy, Rutgers, The State University of New Jersey, 136 Frelinghuysen Road, Piscataway, NJ 08854, USA

<sup>3</sup> Department of Physics & Astronomy, The State University of New York, Stony Brook, NY 11794, USA

<sup>4</sup> EMAT, Department of Physics, University of Antwerp, Groenenborgerlaan 171, 2020 Antwerp, Belgium

<sup>5</sup> Brookhaven National Laboratory, Upton, NY 11973, USA

<sup>6</sup> Department of Physics, University of California, San Diego, La Jolla, CA 92093-0319, USA

## Abstract

Recently  $\text{CsTlCl}_3$  and  $\text{CsTlF}_3$  perovskites were predicted theoretically to be potential superconductors. The synthesis of these two new compounds, together with complete characterizations of the samples is reported for the first time.  $\text{CsTlCl}_3$  is obtained as orange single crystals and  $\text{CsTlF}_3$  as light brown powders. The structure of the samples was determined by electron diffraction, synchrotron powder x-ray diffraction and single crystal x-ray diffraction.  $\text{CsTlCl}_3$  is obtained in two different polymorphs: a tetragonal phase (space group  $I4/m$ ), similar to  $\text{CsAuCl}_3$ , with  $\text{Tl}^{1+}$  and  $\text{Tl}^{3+}$  in two different crystallographic positions, and therefore with charge ordering;  $\text{CsTlCl}_3$  was also obtained as a cubic and less distorted phase (space group  $Fm\text{-}3m$ ), also with two different positions for  $\text{Tl}^{1+}$  and  $\text{Tl}^{3+}$ .  $\text{CsTlF}_3$  was obtained as a cubic phase with space group  $Fm\text{-}3m$  and  $\text{Tl}^{1+}$  and  $\text{Tl}^{3+}$  in two unique sites. All three compounds are paramagnetic; according to theory, hole doping and high pressure are required to achieve superconductivity in the  $\text{CsTlX}_3$  (X = F, Cl) cubic perovskites. The mixed  $\text{Tl}^{1+}$  and  $\text{Tl}^{3+}$  valence has been confirmed by x-ray absorption spectroscopy. The optical gap has been determined by spectroscopic techniques to be  $\sim 2.5$  eV, in reasonable agreement with that calculated by first-principles density functional

theory (~2.1 eV). The theoretical design and the experimental validation of  $\text{CsTlF}_3$  and  $\text{CsTlCl}_3$  cubic perovskites is an extraordinary starting point since, in theory, superconductivity in these materials can be achieved in cubic phases.

**Keywords:** superconductivity, mixed valence, charge order,  $\text{CsTlCl}_3$ ,  $\text{CsTlF}_3$ ,  $\text{CsAuCl}_3$ ,  $\text{BaBiO}_3$ ,  $\text{Ba}_{1-x}\text{K}_x\text{BiO}_3$ ,  $\text{Ba}_{1-x}\text{Pb}_x\text{BiO}_3$ .

## Introduction

The discovery of high- $T_C$  superconductivity in mixed-valent systems such as  $\text{La}_{2-x}\text{Ba}_x\text{CuO}_4$ <sup>1,2</sup> and  $\text{Ba}_{1-x}\text{K}_x\text{BiO}_3$ ,<sup>3,4</sup> have attracted great interest in search for new superconducting materials; in particular in compounds with perovskite-type structure.  $\text{BaBiO}_3$  becomes superconducting when it is doped as  $\text{Ba}_{1-x}\text{K}_x\text{BiO}_3$  ( $x \sim 0.4$ ) and  $\text{BaBi}_{1-x}\text{Pb}_x\text{O}_3$  ( $x \sim 0.3$ ).<sup>4,5</sup> In the parent compound  $\text{BaBiO}_3$ , formally  $\text{Bi}^{4+}$  disproportionates into  $\text{Bi}^{3+}$  (lone pair  $6s^2$ ) and  $\text{Bi}^{5+}$  ( $6s^0$ ), which alternate at the B site, generating distortions from the ideal perovskite structure. Since the  $6s$  orbital has a large radial extension, the Bi-O bond distance is longer for  $\text{Bi}^{3+}$ -O than for  $\text{Bi}^{5+}$ -O (due to the localized  $6s$  orbital).<sup>6</sup> When  $\text{BaBiO}_3$  is doped, the difference between the two Bi-O bond lengths decreases and superconductivity emerges, when the structural distortions are completely suppressed.<sup>7</sup> These observations suggest that superconductivity in the  $\text{BaBiO}_3$  system is mediated by the same mechanism that is responsible for the charge disproportionation of the mixed-valent cations. However, superconductivity has not been found in other similar mixed-valent systems. For example, in  $\text{Cs}_2\text{SbCl}_6$  the absence of superconductivity is attributed to the large activation energy required for charge disproportionation, due to the difference in bond lengths (Sb-Cl) between  $\text{Sb}^{3+}$  and  $\text{Sb}^{5+}$  sites.<sup>8</sup> Further, the compounds  $\text{CsAuX}_3$  ( $\text{X} = \text{Cl, Br, I}$ ) with  $\text{Au}^{1+}$  and  $\text{Au}^{3+}$  mixed-valent states,<sup>9-11</sup> and exactly one hole per site are semiconductors (at low pressure) with a large band gap.<sup>12</sup> Although, the conductivity of  $\text{CsAuX}_3$  increases by several orders of magnitude at high pressures (a few GPa), nevertheless, superconductivity, has not been found thus far.<sup>13-16</sup> In  $\text{CsAuX}_3$ , at ambient pressure, the activation barrier for direct electron pair transfer is very large. Increased pressure forces the geometric differences between different oxidation states to become smaller, decreasing the activation barrier and moving from an insulator state to a metallic state. Although  $\text{CsAuX}_3$  are structurally similar to  $\text{BaBiO}_3$  and share a similar mixed-valence of the B cations, the absence of superconductivity in the former phases suggests that charge disproportionation is not the sole consideration for superconductivity.

Recently, the high temperature superconductivity in a large family of materials including  $(\text{Ba},\text{K})\text{BiO}_3$  and electron-doped  $\text{HfNCl}$ <sup>17,18</sup> was explained by a correlation-enhanced strong

electron-phonon coupling mechanism.<sup>19</sup> This coupling in  $\text{CsAuCl}_3$  was found to be weak, accounting for the absence of superconductivity in agreement with experiments. Nevertheless, based on the correlation-enhanced strong electron-phonon coupling mechanism, it was predicted that high temperature superconductivity can be found in the  $\text{CsAuX}_3$ -like perovskites:  $\text{CsTlF}_3$  and  $\text{CsTlCl}_3$ .<sup>20</sup> Both compounds were predicted to be isostructural with  $\text{BaBiO}_3$ , share the same valence electron count as  $\text{BaBiO}_3$ , and retain essentially the same band structure near the Fermi level. With these similarities,  $\text{CsTlF}_3$  and  $\text{CsTlCl}_3$  were shown theoretically to be superconducting with some hole doping and under pressure (required to suppress the structural distortions). The critical superconducting temperature ( $T_C$ ) was predicted to be  $\sim 30$  K for  $\text{CsTlF}_3$  and  $\sim 20$  K for the Cl analogue, under an optimal hole doping level ( $\sim 0.35/\text{f.u.}$ ) and moderate pressures (between  $\sim 10$  and  $\sim 2$  GPa, respectively).<sup>20</sup>

There are two important aspects that are taken into account when theoretically designing these materials: the compounds must be energetically favorable among all possible competing phases with the Cs-Tl-X (X = F, Cl) composition and the proposed structure must be dynamically stable. The designed materials should form in real experiments, if these two criteria are satisfied. Both compounds would be formed in the perovskite ( $\text{ABO}_3$ ) structure with  $\text{Cs}^+$  cations in the A site and  $\text{Tl}^{1+}$  and  $\text{Tl}^{3+}$  in the B site;  $\text{Tl}^{1+}$  and  $\text{Tl}^{3+}$  could order in two B and B' sites, forming a double perovskite  $\text{Cs}_2\text{Tl}^{1+}\text{Tl}^{3+}\text{X}_6$ , partially order, or disorder in the simple  $\text{CsTlX}_3$  perovskite with one B site for both  $\text{Tl}^{1+}$  and  $\text{Tl}^{3+}$  cations.

In this work, we were able to prepare these two theoretically designed novel materials with thallium formally in mixed (1+/3+) oxidation state, and thereby open a new field of research in the exploration of new superconductors. We have characterized both materials ( $\text{CsTlX}_3$ , with X = F, Cl), determined their crystallographic structures and confirmed mixed-valent  $\text{Tl}^{1+/\text{3}+}$  in both compounds. The next challenge is to optimally dope (and put under high pressure) these materials to find superconductivity.

## Experimental Section

*Synthesis of CsTlCl<sub>3</sub>:* the compound was prepared in polycrystalline form by two different methods of synthesis. First a precursor of Cs<sub>2</sub>TlCl<sub>5</sub> was prepared by dissolving 3 g of CsCl in 10 ml of HCl (37 %) and 0.3 g of Tl<sub>2</sub>O<sub>3</sub> in 3 ml of HCl (37 %). When the Tl solution is added to the Cs one, a white-yellow precipitate appeared immediately (the powder x-ray diffraction (PXD) identifies this precipitate as CsCl, mainly, with other amorphous products). When 100 ml of water were added to this precipitate, it dissolved and some white crystallized material appeared, which was identified as Cs<sub>2</sub>TlCl<sub>5</sub>·H<sub>2</sub>O (Fig. S1a). In the second step of the synthesis stoichiometric quantities of the starting materials Cs<sub>2</sub>TlCl<sub>5</sub>·H<sub>2</sub>O + TlCl were mixed inside a glove box (to avoid contact of TlCl with air) and ground; the mixture was placed in a silica tube, sealed under vacuum and heated to 600 °C for 12 hs with a heating and cooling rate of 3 °C/min. The PXD pattern of the obtained material (Fig. 1a) is characteristic of a distorted perovskite with tetragonal symmetry similar to Cs(Au<sup>1+</sup>)<sub>1/2</sub>(Au<sup>3+</sup>)<sub>1/2</sub>Cl<sub>3</sub>. Henceforth, this CsTlCl<sub>3</sub> tetragonal phase will be designated as CsTlCl<sub>3</sub>-t. The products are obtained as yellow-orange crystals of several millimetres, as shown in the inset of Fig. 1a.

An alternative method of synthesis with TlCl, CsCl and TlCl<sub>3</sub>·xH<sub>2</sub>O as starting materials was also attempted. All the preparation steps were carried out inside the glove box to avoid the decomposition of TlCl and TlCl<sub>3</sub>·xH<sub>2</sub>O. The synthesis of the final product was also carried out in a silica tube sealed under vacuum and the final temperatures were the same as in the synthesis described above. CsTlCl<sub>3</sub> is also obtained by this alternative method, and the obtained material has the same tetragonal structure, CsTlCl<sub>3</sub>-t (Fig. S2a and S2b show the comparison of the PXD using both techniques). The synthesis is always reproducible by either of the preparation techniques described above. To test the presence of water in the final product, some powder CsTlCl<sub>3</sub>-t material was heated in air to 300 °C and the residual obtained has the same PXD pattern as before heating (Fig. S2c).

A different phase of CsTlCl<sub>3</sub> is obtained when anhydrous Cs<sub>2</sub>TlCl<sub>5</sub> is used as starting material instead of Cs<sub>2</sub>TlCl<sub>5</sub>·H<sub>2</sub>O. In this case, the previously formed precursor Cs<sub>2</sub>TlCl<sub>5</sub>·H<sub>2</sub>O, was heated at 150 °C for 30 minutes to form anhydrous Cs<sub>2</sub>TlCl<sub>5</sub> (Fig. S1b). Cs<sub>2</sub>TlCl<sub>5</sub> was mixed with stoichiometric quantity of TlCl, ground together, placed in a silica tube, sealed under

vacuum and heated to 600 °C for 12 hours. The crystals obtained in this reaction are also yellow-orange, similar in size and shape, but somewhat lighter in color than the other phase. Moreover, this phase has a significantly different structure than the tetragonal ( $\text{CsTlCl}_3\text{-t}$ ) polymorph. It is also a perovskite-based material, but the splitting of many reflections seen in the PXD of  $\text{CsTlCl}_3\text{-t}$  disappears. This new cubic-like perovskite henceforth will be designated as  $\text{CsTlCl}_3\text{-c}$ . Fig. 1 illustrates the PXD of  $\text{CsTlCl}_3\text{-t}$  (Fig. 1a) and  $\text{CsTlCl}_3\text{-c}$  (Fig. 1b), where the difference between the two is illustrated. Thus we have observed the existence of two different phases in the  $\text{CsTlCl}_3$  system and a study of both crystallographic structures is described below. The difference between the two phases appears to be related to the quantity of water present in the starting materials, although no water is found inside the structure. Thus it seems that water is required for the formation of the tetragonal phase. The tetragonal phase forms much easier than  $\text{CsTlCl}_3\text{-c}$ , and unless the starting materials are thoroughly dried, the very stable  $\text{CsTlCl}_3\text{-t}$  phase appears.

*Synthesis of  $\text{CsTlF}_3$*  has also been carried out entirely inside a glove box, in order to avoid contact of the starting materials, as well as the obtained products, with air and moisture. The synthesis must be carried out in two different steps: first the synthesis of one of the starting materials,  $\text{TlOF}$ , which is the source of  $\text{Tl}^{3+}$ ;  $\text{TlOF}$  is required, because  $\text{TlF}_3$  is difficult to prepare, and unstable.  $\text{TlOF}$  was prepared by adding  $\text{Tl}_2\text{O}_3$  to a solution of HF (37 %). After some minutes the characteristic brown color of  $\text{Tl}_2\text{O}_3$  turned into the characteristic green color of  $\text{TlOF}$ .

The second and final step of the procedure is the reaction:  $\text{CsF} + \frac{1}{2}\text{TlF} + \frac{1}{2}\text{TlOF} + x\text{C}_2\text{F}_4$ . Tetrafluoroethylene ( $\text{C}_2\text{F}_4$ ) is required for the successful formation of  $\text{CsTlF}_3$  (without  $\text{C}_2\text{F}_4$  there are insufficient F ions to form the desired compound). These starting materials were pressed into a pellet and covered by a Pt foil, and then heated in an evacuated sealed silica tube at 500 °C for 12 hs with a heating rate of 5 °C/min and a cooling rate of 3 °C/min. The Pt foil is required to avoid contact of the starting materials with the silica tube, and to avoid the competing reaction, producing  $\text{Cs}_2\text{SiF}_6$ , instead of the desired product. Another detail of the experimental procedure is that  $\text{C}_2\text{F}_4$  must be added in small pieces and included together with the pellet of the starting materials under the Pt foil. If  $\text{C}_2\text{F}_4$  is added prior to the grounding, and pelletized with the other

components, the silica tube explodes in the furnace. The reaction succeeds for quantities of  $C_2F_4$  around  $x = 2$  to 3. The product formed was washed in methanol to eliminate  $TlCl$  and  $CsCl$  impurities. The PXD pattern of this sample with a cubic perovskite structure is shown in Fig. 2.

The PXD characterization of the samples was carried out with  $Cu\ K_{\lambda}$ ,  $\lambda = 1.5406\ \text{\AA}$  on a Bruker X-ray diffractometer. For the structural refinement of  $CsTlF_3$  and  $CsTlCl_3$ -t, synchrotron x-ray diffraction (SPXD) data were collected at room temperature at the X16C beam line in the Brookhaven National Laboratory. About 0.2 mg of sample was loaded inside a capillary; a collecting time of 2 hs was required for each pattern. Refinements carried out with TOPAS-Academic.<sup>21</sup>

The structure determination of the tetragonal and cubic phases of  $CsTlCl_3$  were performed by use of single-crystal x-ray data (SCD) collected on a Bruker Smart APEX CCD diffractometer with graphite monochromatized  $Mo\ K_{\lambda}$  radiation ( $\lambda = 0.71073\ \text{\AA}$ ) at 100 K. The data were corrected for Lorenz effects and polarization, and absorption, the latter by a multi-scan (SADABS)<sup>22</sup> method. The structures were based on the known model from Ref. 9. All atoms were refined by use of JANA2006<sup>23</sup> program and anharmonic ADP or by use of SHELXL97<sup>24</sup> and harmonic ADP and split sites for Cs and Tl atoms. Crystallographic data is given in the supporting information.

Samples for electron microscopy were prepared by dispersing crushed single crystals in ethanol and depositing a few drops of this solution on a holey carbon grid. Selected area electron diffraction (SAED) patterns were obtained on a Philips CM20 transmission electron microscope (TEM) equipped with a CCD camera.

The magnetic measurements were performed in a commercial superconducting quantum interference device magnetometer (SQUID). The *dc* magnetic susceptibility data were collected in the  $1.8 \leq T \leq 400$  K range under an applied magnetic field of 10000 Oe. Isothermal magnetization curves were obtained in magnetic fields up to 7 T at  $T = 1.8$  K.

The XAS measurements were made in both fluorescence and transmission modes on beamline X-19A at the National Synchrotron Light Source (NSLS) at Brookhaven National Laboratory using a Si(111) double-crystal monochromator.<sup>25,26</sup> The relative energy calibrations were made by the simultaneous-run standard method with a Tl<sub>2</sub>O<sub>3</sub> standard for the Tl-L<sub>3</sub> measurements. The low energy Cl-K edge measurements were performed in the fluorescence mode in a He-atmosphere with separate standard scans. The data were processed with the standard linear pre- and post-edge background subtraction. By convention, the absorption coefficient ( $\mu$ ) is normalized to 1.0 over an average energy region well above the edge.

## Results and Discussion

The synthesis of these compounds is not trivial, due to several factors. First, thallium is extremely toxic; hence extreme precaution is required in all the procedures. Second, especially the fluorides are also very reactive (unstable), and thus the synthesis is often unsuccessful. For instance, the fluorides attack the Pt foil, hence a fresh Pt foil must be used in each experiment. We have tried the synthesis with other metal foils instead of Pt, and many alternative procedures without success.

### *Crystal Structure*

#### *CsTlCl<sub>3</sub>-c*

The PXD pattern (Fig. 1b) of CsTlCl<sub>3</sub>-c, is similar to the high pressure cubic phase of CsAuCl<sub>3</sub>.<sup>13</sup> All the features of the PXD pattern are consistent with the cubic symmetry and are in excellent agreement with the PXD pattern calculated from the SCD refinement (see below). To help solve the structure, the SAED of CsTlCl<sub>3</sub>-c was undertaken. The sample decomposed when the electron beam was focussed into a high intensity spot; thus it was not possible to perform imaging (HRTEM, HR-STEM) and convergent-beam electron diffraction (CBED). What can be done in this case is SAED, which allows the determination of the unit cell parameters and provides evidence for the possible space groups based upon observed reflection conditions.

SAED was performed on the crushed sample containing inter-grown single crystals from the melt. Electron diffraction patterns were taken from different crystallites by tilting around different reciprocal lattice directions. All patterns could be indexed with the cell parameters determined from the PXD data, and space group  $Fm\text{-}3m$ , with  $a = 10.84 \text{ \AA}$ . Representative SAED patterns are shown in Fig. 3.

The refinement of the  $\text{CsTlCl}_3\text{-c}$  structure was carried out with SCD data collected at 100K. The structural refinements were performed using JANA2006. The PXD pattern calculated from this refinement is essentially identical to that calculated from the SCD data, and is illustrated in Fig. 4. The initial SCD model was based upon the “conventional” model (as in Ref. 9) of a cubic double perovskite with  $Fm\text{-}3m$  space group and the atoms in these positions:  $\text{Cs}^+$  at A ( $\frac{1}{4} \frac{1}{4} \frac{1}{4}$ ),  $\text{Tl}^{3+}$  at B (0 0 0),  $\text{Tl}^{1+}$  at B' ( $\frac{1}{2} 0 0$ ) and  $\text{Cl}^-$  anions over ( $x 0 0$ ) with  $x \sim 0.239$ . However, the occupancy of the  $\text{Cl}^-$  anion in that site, Cl1, was found to be deficient by about 16% and a second Cl site, Cl2, of approximate occupancy 16% was found 1.9  $\text{\AA}$  away, at ( $x = 0 y = z = 0.169$ ). Large residuals in the difference-electron-density maps in the vicinity of Tl at B' ( $\frac{1}{2} 0 0$ ) and Cs at A ( $\frac{1}{4} \frac{1}{4} \frac{1}{4}$ ) indicated significant disorder around these two positions. Two different models were used to explain this disorder: a) use of Gram-Charlier anharmonic parameters up to six orders, and the final atomic parameters from a JANA2006 refinement using anharmonic ADP are shown in Table 1, with average bond distances shown in Table 2; b) use of a split atom model in program SHELXL to quantify the displacements of the Cs and Tl atoms in sites A and B', respectively. The Cs atom was placed at the A site and also at 2 unique sites nearby, yielding a regular polygon with 10 vertices of partial Cs atoms about the partial Cs atom at ( $\frac{1}{4} \frac{1}{4} \frac{1}{4}$ ); the average distance from ( $\frac{1}{4} \frac{1}{4} \frac{1}{4}$ ) was approximately 0.5  $\text{\AA}$ . A similar procedure for the Tl in B' site yielded a regular polygon with 18 vertices of Tl atoms spaced evenly about 0.9  $\text{\AA}$  from the partial Tl atom in the B' site ( $\frac{1}{2} 0 0$ ). The atomic parameters obtained from the refinement using this second model are shown in the supporting information (Tables S2 and S3) and the bond distance ranges indicated by the displacements of A and B' site atoms from the SHELXL split atom with harmonic ADP model are shown in Table S4. Both types of refinements have been previously reported in other, similarly disordered systems, such as  $\text{Ni}_{1+\delta}\text{Sn}$  or  $\text{LaNi}_5$ .<sup>27-29</sup>

In both models the occupancy of Tl in the B' site was found to have less than full occupancy, namely 0.68 with the intensity weighting scheme based upon  $[\sigma(I) + 0.1*I^4]$  in JANA2006; other weighting schemes gave different results, but the occupancy was always found to be deficient and in the range 0.65 to 0.75. Thus, the B' site appears to contain some vacancies and requires the presence of both  $Tl^{1+}$  and  $Tl^{3+}$  for charge balance, but is mainly occupied by  $Tl^{1+}$ . This result would explain the slightly shorter  $Tl(B')-Cl1$  distances found in both models (Table 2 and Table S2) compared with the expected bond distance of 3.31 Å from Shannon radii sum,<sup>30</sup> while  $Tl(B)-Cl$  distances match very well with six-coordinate  $Tl^{3+}$  cations, 2.70 Å. Occurrences of vacancies in other perovskite-like chlorides (e.g.,  $Cs_2MCl_6$  with  $K_2PtCl_6$  structural type in space group  $Fm-3m$ ) have been reported, and take place when M is a tetravalent cation, such as Sn, Ta, Re, W, etc.<sup>31-34</sup> We have also investigated the possible existence of oxygen over either  $Cl^-$  site, and  $O^{2-}$  did not refine nearly as well as  $Cl^-$  in these positions, and gave unrealistic metal-oxide bond lengths. A second crystal from another synthesis gave similar SCD results, with use of either the JANA2006 or the SHELXL refinement described above.

Further examination of the two sites for the  $Cl^-$  ions reveals that only Cl1 atoms at site (0.239 0 0) are close enough to the Tl atoms of site B' to form bonds, but both Cl1 and Cl2 atoms form metal-chloride bonds (but not at the same time) to the  $Cs^+$  in A site and the  $Tl^{+3}$  in B site. The appearance of this second  $Cl^-$  at the interstitial site (0 0.169 0.169) has been also observed in some oxygen-containing double perovskites with large B-site cations (as  $Tl^{1+}$  is in our case), such as  $Sr_2(Sr_{1-x}M_{1+x})O_6$  (B = Nb, Ta) and  $Sr_2MSbO_6$  (M = Ca, Sr, Ba),<sup>35-38</sup> The large B-site cation causes non-harmonic atomic displacements that drives some oxygen to interstitial site and leaves oxygen vacancies in the original positions. The existence of interstitial oxygen yields short bond distances between those O atoms and the large A-site and B-site cations, for example, Sr-O and Ba-O distances of 2.311 and 1.964 Å in  $Sr_2BaSbO_{5.5}$ . In perhaps an analogous way, the large B'-site  $Tl^{1+}$  (i.r.  $Tl^{1+}$  (VI) = 1.5 Å)<sup>30</sup> requires some  $Cl^-$  to locate in the interstitial site in  $CsTlCl_3-c$ , which gives rise to an extra set of  $Cs-Cl2$  and  $Tl^{+3}(B)-Cl2$  bond lengths. As a result, the Tl in site B' is significantly further from Cl2 (4.14 Å) than Cl1 (2.84 Å).

We have performed SCD together with SPXD and SAED in an attempt to solve the complex structure of the  $\text{CsTlCl}_3\text{-t}$  compound. The PXD pattern is similar to the previously reported  $\text{CsAuCl}_3$  compound, with mixed valence  $\text{Au}^{1+}/\text{Au}^{3+}$  and a distorted cubic perovskite structure in the tetragonal space group ( $I4/mmm$ ).<sup>10,39</sup> However many additional, but small features were observed in the PXD of  $\text{CsTlCl}_3\text{-t}$ , which could not be accounted for by space group  $I4/mmm$ , or other space groups appropriate for compounds similar to  $\text{CsAuCl}_3$  with similar cell parameters.

SAED was performed on the crushed sample containing inter-grown single crystals from the melt. The same sensitivity to the electron beam occurred for this sample as for  $\text{CsTlCl}_3\text{-c}$ . Several tilt series of SAED data were taken from different crystallites in the sample. The sample showed clear superstructure reflections, as was evidenced from the two most prominent zones shown in Fig. 5, which originated from two separate pieces. To index all reflections, a supercell was needed, with cell parameters approximately  $a \approx 17.0 \text{ \AA}$ ,  $b \approx 17.0 \text{ \AA}$ , and  $c \approx 11.0 \text{ \AA}$ . Any differences between the lengths of  $a$  and  $b$  are too small to distinguish with TEM. The relationship between this supercell and the cell of a tetragonal double perovskite of formula  $\text{Cs}_2\text{Tl}^{1+}\text{Tl}^{3+}\text{Cl}_6$  with subcell parameters refined with our PXD data as  $\sim a = b = 7.7 \text{ \AA}$ , and  $c = 11.0 \text{ \AA}$  and space group  $I4/m$  is given by the transformation matrix  $P = \begin{bmatrix} 1 & -2 & 0 \\ 2 & 1 & 0 \\ 0 & 0 & 1 \end{bmatrix}$ , which yields a

5-fold increase in the unit cell volume and a resultant tetragonal superlattice of  $5^{1/2}\mathbf{a} \ 5^{1/2}\mathbf{b} \ \mathbf{c}$ . From the obtained zones, the reflection conditions  $hkl: h + k + l = 2n$  and  $hk0: h + k = 2n$  indicated an I-centered unit cell, while the reflection conditions  $hh0: h = 2n$  and  $00l: l = 4n$  were ruled out. This leaves as possible extinction symbols I--- and I-c-, and therefore 11 possible space groups agreeing with these extinction symbols. To reduce the number of possible space groups, the intensity distribution in the [001] zone shown in Fig. 5, was taken into account. The intensity distributions in SAED patterns can only be considered with great care, because aside from the unavoidable addition of inversion symmetry, also imperfections in orientation of the crystal can cause changes in the intensities. However, for the following considerations, only a specific set of reflections were considered, where the inequalities are very obvious and unmistakable within the following reflection set: 240, -240, 2-40, -2-40, 420, -420, 4-20, -4-20.

Among these, the reflections -240, 2-40, -4-20, 420 were found to be equivalent according to the experimental SAED patterns, while the other four reflections in the set are very clearly not equivalent to these. This inequivalence allows the elimination of 8 out of 11 of the remaining possible space groups,<sup>40</sup> since for I4, I-4, and I4/m the hk0 are only equivalent to -h-k0, -kh0, k-h0, which is in agreement with the experimental observation, while for the other 8 space groups also the other four reflections (h-k0, -hk0, kh0, -k-h0) should be equivalent, which is not in agreement with the experimental observations. No other extinctions were observed, so that the only possible space groups appeared to be I4, I-4, and I4/m. To decide between I4, I-4, and I4/m CBED should be used, since they do not differ in reflection conditions, only in point group, but on this material performing CBED is impossible, because the material immediately decomposes under the intense beam required for CBED.

In addition, the SPUDS program<sup>41</sup> was used to predict the probable space group. The program works by distorting the structure to minimize the global instability index (GII), while maintaining the rigidity of the octahedral network in the perovskite structure. The stability of perovskite compositions with different atoms, symmetry, tilt systems and structure can be evaluated by comparing the GII. The GII value is typically < 0.1 valence units (v.u.) for unstrained structures and as large as 0.2 v.u. in a structure with lattice induced strains. Crystal structures with a GII > 0.2 v.u. are typically found to be unstable, and reports of such structures are usually found to be incorrect. The predicted space groups with GII < 0.2 v.u for both  $\text{Cs}_2\text{Ti}^{1+}\text{Ti}^{3+}\text{Cl}_6$  ( $\text{CsTiCl}_3$ ) and  $\text{Cs}_2\text{Ti}^{1+}\text{Ti}^{3+}\text{F}_6$  ( $\text{CsTiF}_3$ ) phases are: Pn-3 ( $a^+a^+a^+$ ), P2<sub>1</sub>/n ( $a^-b^+a^-$ ), R-3 ( $a^-a^-a^-$ ), I2/m ( $a^0b^-b^-$ ), P4/mnc ( $a^0a^0c^+$ ), I4/m ( $a^0a^0c^-$ ) and Fm-3m ( $a^0a^0a^0$ ). All these space groups require one site (e.g., B') with only  $\text{Ti}^{1+}$  and another site (e.g., B) with only  $\text{Ti}^{3+}$ . Thus, taking into account both the SPUDS and SAED results, only I4/m would appear to be suitable for  $\text{CsTiCl}_3$ -t. By SCD we observed the same cell as by SAED, with a tetragonal space group and cell parameters  $a \approx b \approx 17.0 \text{ \AA}$  and  $c \approx 11.0 \text{ \AA}$ . However, similar disorder as in  $\text{CsTiCl}_3$ -c is observed on the  $\text{Ti}^{1+}$  and  $\text{Cs}^{1+}$  positions of  $\text{CsTiCl}_3$ -t, which are expected to be at least five times more numerous than for the cubic phase of 1/5<sup>th</sup> the volume. Thus, as in the case of the cubic phase, the resolution of the tetragonal structure will likely require significant displacements of the atoms about their central sites computed with the matrix above, and anharmonic thermal

parameters should aid in the model description. We are currently making progress toward a satisfactory model in this manner. Additionally, we have some indications that there may be correlations between the 5-fold transformation to supercell and the positions and/or occupancies of the atom sites in the supercell. Fig. 6 shows a Pawley fit to the  $\text{CsTlCl}_3\text{-t}$  compound using SPXD. The lattice parameters are  $a = 17.2487(5)$  Å and  $c = 11.1003(4)$  Å, and the extinction symbol  $I---$  is used. In conjunction with the electron diffraction result that the Laue class is  $4/m$ , which restricts to space groups  $I4$ ,  $I-4$ , and  $I4/m$ . There is an impurity of  $\text{TlCl}$ , which has  $\text{CsCl}$  structure and cell parameter  $a = 3.846$  Å.

### $\text{CsTlF}_3$

The PXD is similar to a previously reported fluoride,  $\text{CsSrF}_3$  with very similar cell parameters.<sup>42</sup> The crystallographic structure of  $\text{CsTlF}_3$  was studied by SPXD. The structure was first refined with the space group determined for  $\text{CsSrF}_3$ ,  $Pm-3m$ , and it was also refined with the space group  $Fm-3m$ , which contains two different Tl sites. The Rietveld fit with space group  $Fm-3m$  ( $R_{wp} = 9.8\%$ ) appears to be slightly better than with  $Pm-3m$  ( $R_{wp} = 9.9\%$ ). The refined parameters in  $Fm-3m$  are  $a = 9.5449(1)$  Å, the position of F (0.277(1), 0, 0), and the observed Tl-F distances 2.12(1) Å and 2.65(1) Å, consistent with  $\text{Tl}^{3+}$  and  $\text{Tl}^{1+}$  distances in other phases: e.g.,  $\text{Tl}^{3+}$  in  $\text{Cs}_3\text{TlF}_6$  (2.02 Å)<sup>43</sup> and  $\text{Tl}^{1+}$  in  $\text{TlF}$  (2.4-2.7 Å).<sup>44</sup> The distances are also comparable with those expected from the ionic radii sums<sup>30</sup> of 2.21 Å for  $\text{Tl}^{3+}$ -F (i.r.  ${}^{VI}\text{Tl}^{3+}$ : 0.88 Å and i.r.  ${}^{VI}\text{F}^-$ : 1.33 Å) and 2.83 Å for  $\text{Tl}^{1+}$ -F (i.r.  ${}^{VI}\text{Tl}^{1+}$ : 1.50 Å). Fig. 7 shows the refinement of the structure in the  $Fm-3m$  cubic model with SPXD. A schematic view of the cubic structure of the double perovskite is shown in the inset of Fig. 2. Some of the shoulders near the main peaks can be explained by the presence of impurities:  $\text{Cs}_3\text{TlF}_6$  ( $I4/mmm$ )<sup>45</sup> 14 wt %,  $\text{Tl}_2\text{O}_3$  ( $Ia-3$ ) 6 %,  $\text{CsO}_2$  ( $I4/mmm$ ) 2 % and  $\text{TlF}$  ( $Pm2a$ ) 1 %.

The discovery of cubic structures in  $\text{CsTlF}_3$  and  $\text{CsTlCl}_3\text{-c}$  is a good starting point for superconductivity since, in theory, superconductivity in these phases could only be achieved in cubic perovskites.<sup>20</sup>

### *Magnetic Measurements*

Fig. 8 shows that  $\text{CsTlCl}_3\text{-t}$ ,  $\text{CsTlCl}_3\text{-c}$ , and  $\text{CsTlF}_3$  are all paramagnetic. In Fig. 8a, we plot the temperature dependence of the susceptibility ( $\chi = M/H$ ) of these three materials measured with a *dc* applied field  $H = 10000$  Oe. The low temperature susceptibility of each sample contains a Curie-Weiss like contribution, which becomes much smaller than the other components of the susceptibility by  $\sim 50$  K. It is the non-Curie-Weiss component, however, that varies strongly between the different materials, and indeed  $\chi$  is an order of magnitude larger in the cubic phase of  $\text{CsTlCl}_3$  than in the tetragonal one. Because these compounds are insulators, this component is likely Van Vleck in origin. The susceptibility of all three compounds undergoes a gentle decrease as the temperature increases to 300 K.

Fig. 8b displays magnetic isotherms of  $\text{CsTlCl}_3\text{-t}$ ,  $\text{CsTlCl}_3\text{-c}$ , and  $\text{CsTlF}_3$  collected at  $T = 1.8$  K. As was the case with the susceptibility above, the shape of these curves is consistent with two components, one that is linear with field and a second that saturates. As shown in the figure, we have modelled these components by the sum of a linear term with a Brillouin function, the latter of which is derived from local moment paramagnetism. Accordingly, the saturated component of the isotherms of  $\text{CsTlCl}_3\text{-t}$  and  $\text{CsTlF}_3$  can be described by  $8.8 \cdot 10^{-4}$  and  $1.1 \cdot 10^{-3} S = 5/2$  moments per formula unit, respectively. The magnetization of the  $\text{CsTlCl}_3\text{-c}$  cubic phase saturates more rapidly with field and can be described by  $2.2 \cdot 10^{-3} S = 9/2$  moments per formula unit. The small magnitude of these values suggests that the saturated magnetization as well as the Curie-like tail in the susceptibility stem from the presence of trace magnetic impurities.

### *X-ray Absorption Spectroscopy*

Tl commonly occurs in  $\text{Tl}^{1+}$  and  $\text{Tl}^{3+}$  valence states, the latter of which involves two 6s-orbital holes. The Tl-L<sub>3</sub> edge XAS signature of  $\text{Tl}^{1+}$  to  $\text{Tl}^{3+}$  change is a chemical shift of the main edge to higher energy and the appearance of a shoulder pre-edge feature due to transitions into the empty 6s hole states.<sup>25</sup> These same signatures are well known at the Bi-L<sub>3</sub> edge to evidence the  $\text{Bi}^{3+}$  to  $\text{Bi}^{5+}$  change.<sup>26,46,47</sup> In Fig. 9a the Tl-L<sub>3</sub> edge spectra of  $\text{CsTlCl}_3\text{-t}$  and  $\text{CsTlCl}_3\text{-c}$  are

compared to those of  $\text{Ti}^{1+}$  and  $\text{Ti}^{3+}$  standards. Assigning the nominal chemical shift as the energy where the normalized absorption coefficient value first rises to the  $\mu = 0.5$  value; the chemical shifts of  $\text{CsTiCl}_3\text{-t}$  and  $\text{CsTiCl}_3\text{-c}$  are clearly intermediate between those of  $\text{Ti}^{1+}$  and  $\text{Ti}^{3+}$  standards supporting their intermediate valence. The disparity between the energies of the  $\mu = 0.5$ , chemical shift points of the  $\text{Ti}^{3+}$  standards,  $\text{Cs}_2\text{TiCl}_5$  and  $\text{Ti}_2\text{O}_3$  underscore the qualitative nature of the inference of the intermediate valence of both  $\text{CsTiCl}_3$ .

In Fig. 9b the pre-edge region of the spectra from the previous figure are plotted on an expanded scale with the  $\text{CsTiCl}_3\text{-t}$  spectrum being left out since it is essentially identical to that of  $\text{CsTiCl}_3\text{-c}$ . The first point to note is that the  $\text{Ti}^{1+}\text{Cl}$  spectrum exhibit a monotonic concave upward curvature over the entire pre-edge region, consistent with the absence of any  $6s$  hole states ( $6s^2$ ). In contrast the  $\text{Ti}^{3+}$  standards manifest pronounced pre-edge shoulder features consistent with the presence of two  $6s$ -orbital holes ( $6s^0$ ). In the  $\text{CsTiCl}_3\text{-c}$  spectrum one can discern a clear, albeit not dramatic, shoulder feature supporting the presence of  $6s$  hole states and a valence state intermediate between  $\text{Ti}^{1+}$  and  $\text{Ti}^{3+}$ . To emphasize the presence of the shoulder feature in  $\text{CsTiCl}_3\text{-c}$ , a sp line fit to the data above and below this feature has been subtracted (as a background) to obtain an estimate of just the shoulder feature portion (denoted  $\Delta\mu$ ). This  $\Delta\mu$  shoulder feature has been plotted in the bottom of Fig. 9b (see right hand plot scale). Thus the conclusion that  $\text{CsTiCl}_3$  materials have a valence intermediate between  $\text{Ti}^{1+}$  and  $\text{Ti}^{3+}$  is supported by both the main edge chemical shift and pre-edge  $s$ -feature XAS results.

The results for the  $\text{Ti-L}_3$  edge spectra of  $\text{CsTiF}_3$  along with  $\text{Ti}^{1+}\text{F}$  and  $\text{Ti}^{3+}\text{O}_3$  standards are shown in Fig. 10. The results are similar to those discussed above for the Cl-based material. The chemical shift (i.e. the energy at which  $\mu = 0.5$ ) of  $\text{CsTiF}_3$  is clearly intermediate between  $\text{Ti}^{1+}$  and  $\text{Ti}^{3+}$  standards, again supporting its intermediate valence. The pre-edge region of the spectra is plotted on an expanded scale in the figure inset. The presence of a pronounced pre-edge shoulder in  $\text{CsTiF}_3$  clearly indicates the presence of  $6s$  hole states. The fact that this shoulder in  $\text{CsTiF}_3$  is reduced in magnitude relative to that in  $\text{Ti}^{3+}\text{O}_3$  standard should be noted. This reduction in the  $6s$  hole state shoulder supports an intermediate  $\text{Ti}^{1+}/\text{Ti}^{3+}$  valence for  $\text{CsTiF}_3$ .

Thus again the conclusion that  $\text{CsTlF}_3$  has a  $\text{Tl}^{1+}/\text{Tl}^{3+}$  intermediate valence is supported both by the main edge chemical shift and pre-edges-feature.

In the argument immediately above a  $6s$  hole state feature comparison between compounds involving O and F was used. The fact that they are adjacent in the periodic table lends credence to such a comparison however; critical consideration of  $2p$  to  $3p$  comparisons is necessitated by our data. Comparing the shoulder features in the  $\text{Tl}^{3+}$  standards  $\text{Cs}_2\text{TlCl}_5$  and  $\text{Tl}_2\text{O}_3$  in Fig. 9a and b one notes that the O-compound shoulder is more intense than that in the Cl-compound. Similarly comparing Fig. 10, the shoulder in  $\text{CsTlF}_3$  is also seen to be more intense than that in  $\text{CsTlCl}_3$ . Thus circumstantially it would appear that the  $6s$  hole shoulder feature is possibly systematically more intense in  $2p$  row than in  $3p$  row compounds. The larger spatial extent and hybridization effects of the  $3p$  shell materials would reasonably support this speculation. Further systematic work is required on this proposal.

## First-principles calculations

One of the important characteristics of the compounds described in Refs. 19 and 20 is that the semi-local local density approximation (LDA) and generalized gradient approximation (GGA) within the density functional theory (DFT) framework substantially underestimate the structural distortions and band gaps of the parent compounds, and incorporating non-local correlations (long-range exchange) using HSE-like (*screened*) hybrid functional brings both quantities to much better agreement with experiments. To test this, we have carried out first-principles density functional theory calculations with the VASP code<sup>48</sup> for the cubic  $\text{CsTlCl}_3$  and compare the results with available experiments. In addition to a generalized gradient approximation (PBE version)<sup>49</sup> exchange-correlation functional, a *screened* hybrid functional HSE06<sup>50</sup> has been adopted to account for the non-local correlation/long-range exchange in this compound.

Using the experimental lattice constant  $a = 10.8226 \text{ \AA}$  for  $\text{CsTlCl}_3$ , we relax the structure within the  $\text{Fm-3m}$  space group. The relaxed Cl position ( $x 0 0$ ) is  $x = 0.2392$  from DFT-PBE and  $x = 0.2359$  from DFT-HSE06. Comparing with the experimental value of  $x = 0.2373$ , DFT-HSE06

result agrees better with experiment. Indeed DFT-PBE underestimates the Cl breathing distortion while DFT-HSE06 slightly overestimates it, similar to the case of  $\text{BaBiO}_3$ .

Adopting the experimental crystal structure (lattice constant  $a = 10.8226 \text{ \AA}$  and Cl position (0.2376 0 0)), we compute the total density of states (DOS) and optical conductivity of  $\text{CsTlCl}_3$  and present them in Figs. 11a and b, respectively. As shown in Fig. 11a and b,  $\text{CsTlCl}_3$  is an insulator with a(n) (indirect) band gap of about 1.3 eV (0.6 eV) and an optical gap of about 2.1 eV (1.4 eV), as computed by DFT-HSE06 (DFT-PBE). The calculated band gap by DFT-GGA is much smaller than the DFT-HSE06 value, illustrating the delocalization error of the semi-local nature of the LDA/GGA functional. This delocalization error also has an impact on the positions of the Cl p states, and consequently the peak positions in the optical conductivity. As shown in Fig. 11a, the valence bands near the Fermi level are dominated by Cl p states, peaking at about -3.0 (-2.4) eV in DFT-HSE06 (DFT-GGA). Correspondingly, the first peak position in the optical conductivity is at about 2.1 (1.4) eV (see Fig. 11b). The DFT-HSE06 optical gap agrees reasonably well with the experimental optical gap of about 2.5 eV estimated from the above optical experiments in transmission mode, and is much larger than the result of the corresponding DFT-GGA calculation using the same crystal structure. The above results confirm that  $\text{CsTlCl}_3$  behaves the same way as  $\text{BaBiO}_3$ ,<sup>19</sup> and is another member of the family of the “other high temperature superconductors”.<sup>19</sup>

## Conclusions

Two new compounds,  $\text{CsTlX}_3$  ( $X = \text{F, Cl}$ ), which were theoretically predicted to become superconducting with appropriate doping and under pressure, were synthesized for the first time. Extensive laboratory, synchrotron powder x-ray, single crystal x-ray diffraction and electron diffraction investigations established that both phases are formed in a perovskite structure with two different positions for  $\text{Tl}^+$  and  $\text{Tl}^{3+}$ , suggesting complete or near-complete charge ordering.  $\text{CsTlCl}_3$  forms two different polymorphs depending on the preparation method. These phases are a tetragonal phase ( $I4/m$ ) similar to  $\text{CsAuCl}_3$ , but with a larger unit cell; and a cubic phase with  $Fm\text{-}3m$  space group with some disorder for monocation positions, as well as interstitial  $\text{Cl}^-$

balancing  $\text{Cl}^-$  site vacancies.  $\text{CsTlF}_3$  is obtained as a polycrystalline powder with cubic symmetry in space group  $\text{Fm-3m}$ . X-ray absorption near edge spectroscopy of Tl, in the Cl and F phases, unambiguously confirms the presence of  $\text{Tl}^{1+}$  and  $\text{Tl}^{3+}$ . Both  $\text{CsTlCl}_3$  and  $\text{CsTlF}_3$  are, experimentally and theoretically, insulating and diamagnetic. First-principles calculations of the crystal structure, density of states and optical conductivity of  $\text{CsTlCl}_3$  together with the corresponding experimental observations suggests that non-local correlations/long-range exchange beyond semi-local LDA and GGA functional forms are needed to account for the experimental observations and are fulfilled by adopting a screened HSE06 hybrid functional form. This confirms the previous prediction in Ref. 20 that  $\text{CsTlCl}_3$  (as well as  $\text{CsTlF}_3$ ) is similar to  $\text{BaBiO}_3$  and is another member of the family of the “other high temperature superconductors”. Appropriate doping to introduce holes into the system, and high pressure measurements to search for superconductivity is underway.

## **Acknowledgement**

This work was supported by NSF-DMR-0966829, DOD-VV911NF-12-1-0172 and Rutgers University (BOG) grants. Z.P. Y and G. K. were supported by the AFOSR-MURI program towards better and higher temperature superconductors. Use of the National Synchrotron Light Source, Brookhaven National Laboratory, was supported by the U.S. Department of Energy, Office of Science, Office of Basic Energy Sciences, under Contract No. DE-AC02-98CH10886.

## **Supporting Information Available**

Details of PXD of the precursors and some obtained materials, TGA and DSC analysis, a second model to explain the structure of the cubic  $\text{CsTlCl}_3$ -c phase, Cl-K edge XAS results And the density of states (DOS) and optical conductivity of  $\text{CsTlF}_3$ .

**Table 1.** Final parameters from JANA2006 refinement of CsTlCl<sub>3</sub>-c with Fm-3m space group and cell parameter a = 10.8226(14) Å.

<i>Atom</i>	<i>Cs(I)</i>	<i>Tl(I)</i>	<i>Tl(2)</i>	<i>Cl(1A)</i>	<i>Cl(1B)</i>
<i>Pct Occ</i>	100%	100%	68(5)%	84(4)%	16(4)%
<i>x</i>	1/4	0	1/2	0.2376(10)	0
<i>y</i>	1/4	0	0	0	0.165(4)
<i>z</i>	1/4	0	0	0	0.165(4)
<i>U</i> <sub>11</sub>	0.092(11)	0.0245(11)	0.151(7)	0.028(5)	0.03(2)
<i>U</i> <sub>22</sub>	0.092(11)		0.151(7)	0.049(4)	0.03(2)
<i>U</i> <sub>33</sub>	0.092(11)		0.151(7)	0.049(4)	0.03(2)
<i>U</i> <sub>12</sub>	0		0	0	0
<i>U</i> <sub>13</sub>	0		0	0	0
<i>U</i> <sub>23</sub>	0		0	0	0.01(2)
<i>C</i> <sub>123</sub>	+0.007(7)				
<i>D</i> <sub>1111</sub>	-0.007(5)		-0.03(3)		
<i>D</i> <sub>1122</sub>	0.000(3)		-0.071(10)		
<i>E</i> <sub>11123</sub>	-0.0004(7)				
<i>F</i> <sub>111111</sub>	-0.004(2)		-0.08(2)		
<i>F</i> <sub>111122</sub>	-0.0002(4)		-0.013(2)		
<i>F</i> <sub>112233</sub>	+0.0004(4)		+0.011(4)		

**Table 2.** Bond lengths [Å] for CsTlCl<sub>3</sub>-c.

Cs-Cl1	12x3.828(1)
Cs-Cl2	12x2.97(2)
Tl(B)-Cl1	6x2.58(1)
Tl(B)-Cl2	6x2.59(5)
Tl(B)-Cl2	6x2.59(5)
Tl(B')-Cl1	6x2.83(1)

The values of the distances for the monocation positions, Cs and Tl(B'), are average values, with maximum displacements from their site centers of 0.5 and 0.9 Å, respectively, based upon a SHELXL split atom refinement.

---

## Bibliographic References

- [1] Müller, K. A.; Bednorz, J. G. *Science* **1987**, *237*, 1133-1139.
- [2] Takagi, H. S.; Uchida, S.; Kitazawa K.; Tanaka, S. *Jpn. J. Appl. Phys.* **1987**, *26*, L123.
- [3] Sleight, A. W.; Gillson, J. L.; Bierstadt, P. E. *Solid State Commun.* **1975**, *17*, 27-28.
- [4] Cava, R. J.; Batlogg, B.; Krajewski, J. J.; Farrow, R.; Rupp Jr., L. W.; White, A. E.; Short, K.; Peck, W. F.; Kometani, T. *Nature* **1988**, *332*, 814-816.
- [5] Khan, Y.; Nahm, K.; Rosenberg, M.; Willner, H. *Phys. Status Solidi A* **1977**, *39*, 79-88.
- [6] Cox D.E.; Sleight, A.W. *Solid State Commun.* **1976**, *19*, 969-973.
- [7] Pei, S.; Jorgensen, J. D.; Dabrowski, B.; Hinks, D. G.; Richards, D. R.; Mitchell, A. W.; Newsam, J. M.; Sinha, S. K.; Vaknin, D.; Jacobson A. J. *Phys. Rev. B* **1990**, *41*, 4126-4141.
- [8] Prassides, K.; Day, P.; Cheetham, A. K. *Inorg. Chem.* **1985**, *24*, 545-552.
- [9] Elliot N.; Pauling, L. *J. Am. Chem. Soc.* **1938**, *60*, 1846-1851.
- [10] Tindemans, J. C. M.; Eijndhoven, V.; Verschoor, G. C. *Mater. Res. Bull.* **1974**, *9*, 1667-1670.
- [11] Wells, A.F. Structural InorganicChemistry, third edition, 374 (Clarendon Press, Oxford 1962).
- [12] Keller, R.; Fenner, J.; Holtzapfel, W.B. *Mater. Res. Bull.* **1974**, *9*, 1363-1369.
- [13] Kojima, N.; Hasegawa, M.; Kitagawa, H.; Kikegawa, T.; Shimomura, O. *J. Am. Chem. Soc.* **1994**, *116*, 25, 11368-11374.
- [14] Kitagawa, H.; Sato, H.; Kojima, N.; Kikegawa, T.; Shimomura, O. *Solid State Commun.* **1991**, *78*, 989-995.
- [15] Kojima N.; Kitagawa, H. *J. Chem. Soc. Dalton Trans.* **1994**, *3*, 327-331.
- [16] Wang, S.; Hirai, S.; Shapiro, M. C.; Riggs, S. C.; Geballe, T. H.; Mao, W. L.; Fisher, I. R. arXiv:1205.1077, **2012**.
- [17] Yamanaka, S.; Hotehama, K.; Kawaji, H. *Nature* **1998**, *392*, 580-582.
- [18] Yamanaka, S.; *Annu. Rev. Mater. Sci.* **2000**, *30*, 53-82.
- [19] Yin, Z. P.; Kutepov, A.; Kotliar, G. arXiv:1110.5751, **2011**.
- [20] Yin, Z. P.; Kotliar, G. *EPL* **2013**, *101*, 27002.
- [21] A.A. Coelho, [www.topas-academic.net](http://www.topas-academic.net)
- [22] Bruker-AXS. SADABS, Bruker Nonius area detector scaling and absorption correction, v2.05, Bruker-AXS Inc., Madison, WI, USA **2003**.
- [23] Petricek,V.; Dusek,M.; Palatinus,L. Jana2006. The crystallographic computing system. Institute of Physics, Praha, Czech Republic, **2006**.
- [24] Sheldrick, G. M. SHELXL97, Program for Crystal Structure Refinement, University of Göttingen, Germany, **1997**.
- [25] Huan, G.; Greaney, M.; Greenblatt, M.; Liang G.; Croft, M. *Solid State Ionics* **1988**, *32-33*, 134-140.
- [26] Li, S.; Greenblatt, M.; Jeon, Y.; Chen, J.; Liang G.; Croft, M. *Physica C* **1991**, *173*, 239-244.

[27] Krivoglaz, M.A. *Diffraction of X-rays and Thermal Neutrons in Imperfect Crystals*, Springer, Berlin, **1992**.

[28] Joubert, J.-M.; Cerny, R.; Latroche, M.; Leroy, E.; Guenee, L.; Percheron-Guegan, A.; Yvon, K.; *J. Solid State Chem.* **2002**, *166*, 1.

[29] Leineweber, A.; Oeckler, O.; Zachwieja, U. *J. Solid State Chem.* **2004**, *177*, 936–945.

[30] Shannon, R.D. *Acta Cryst. A* **1976**, *32*, 751-767.

[31] Brill, T. B.; Gearhart, R. C.; Welsh, W. A. *J. Magn. Reson.* **1974**, *13*, 27-37.

[32] Yun, H.; Jang, G.-J. *Acta Cryst. E* **2007**, *63*, i22-i23.

[33] Sperka, G.; Mautner, F.A. *Cryst. Res. Technol.* **1988**, *23*, k109-k111.

[34] Wang, P.; Xu, W.; Zheng, Y.-Q. *Zeitschrift fuer Kristallographie - New Crystal Structures* **2003**, *218*, 25.

[35] Deniard, P.; Caldes, M. T.; Zou, X. D.; Diot, N.; Marchand, R.; Brec R. *International Journal of Inorganic Materials* **2001**, *3*, 1121–1123.

[36] King, G.; Thomas, K. J.; Llobet A. *Inorg. Chem.* **2012**, *51*, 13060–13068.

[37] Caldes, M. T.; Deniard, P.; Zou, X. D.; Marchand, R.; Diot, N.; Brec R. *Micron* **2001**, *32*, 497-507.

[38] Li, M.-R.; Hong S.-T. *Chem. Mater.* **2008**, *20* (8), 2736-2741.

[39] Denner, W.; Schulz, H.; D'Amour, H. *Acta Crystallogr. A* **1979**, *35*, 360–365.

[40] International Tables for Crystallography B, section 1, appendix 1.4.4.

[41] Lufaso, M. W.; Woodward, P. M. *Acta Cryst. B* **2001**, *57*, 725-738.

[42] Wu, G.Q.; Hoppe, R. *Zeitschrift fuer Anorganische und Allgemeine Chemie* **1984**, *514*, 92-98.

[43] Bode, V.H.; Voss, E. *Zeitschrift fuer Anorganische und Allgemeine Chemie* **1957**, *290*, 1-16.

[44] Berastegui, P.; Hull, S. J. *Solid State Chem.* **2000**, *150*, 266-275.

[45] Bode, H.; Voss, E. Z. *Anorg. Allg. Chem.* **1957**, *290*, 1-16.

[46] Yang, T.; Abakumov, A.; Hadermann, J.; Van Tendeloo, G.; Nowik, I.; Stephens, P.; Hemberger, J.; Tsirlin, A.; Ramanujachary, K.; Lofland, S.; Croft, M.; Ignatov, A.; Sun J.; Greenblatt, M. *Chem. Sci.* **2010**, *1*, 751-762.

[47] Heald, S. M.; DiMarzio, D.; Croft, M.; Hegde, M.S.; Li S.; Greenblatt, M. *Phys. Rev. B* **1989**, *40*, 8828-8833.

[48] Kresse G.; Furthmuller, J. *Comput. Mat. Sci.* **1996**, *6*, 15-50.

[49] Perdew, J. P.; Burke, K.; Ernzerhof, M. *Phys. Rev. Lett.* **1996**, *77*, 3865-3868.

[50] Kruckau, A. V.; Vydrov, O. A.; Izmaylov, A. F.; Scuseria, G. E. *J. Chem. Phys.* **2006**, *125*, 224106.

## Figure captions

**Fig. 1:** PXD patterns of  $\text{CsTlCl}_3$  prepared with (a)  $\text{Cs}_2\text{TlCl}_5 \cdot \text{H}_2\text{O} + \text{TlCl}$  as starting materials ( $\text{CsTlCl}_3\text{-t}$ ) and (b)  $\text{Cs}_2\text{TlCl}_5 \text{ anh.} + \text{TlCl}$  ( $\text{CsTlCl}_3\text{-c}$ ). Inset of Fig. 1a: Single crystals of  $\text{CsTlCl}_3\text{-t}$ .

**Fig. 2:** PXD patterns of  $\text{CsTlF}_3$ ; inset is the idealized cubic double perovskite structure of the  $\text{CsTlX}_3$  ( $\text{X} = \text{F}, \text{Cl}$ ) phases.

**Fig. 3:** Representative selected area electron diffraction patterns of  $\text{CsTlCl}_3\text{-c}$ , indexed in the F-centered cell described in the text.

**Fig. 4:** Comparison of (a) experimental PXD of  $\text{CsTlCl}_3\text{-c}$  and (b) Simulation from SCD using whole-site anharmonic ADP model.

**Fig. 5:** Three most prominent zones from the series taken from  $\text{CsTlCl}_3\text{-t}$ . Patterns are indexed in the supercell mentioned in the text.

**Fig. 6:** Pawley fit to  $\text{CsTlCl}_3\text{-t}$  with SPXD. Lattice parameters  $a = 17.2487(5)$  Å and  $c = 11.1003(4)$  Å. Extinction symbol I---.

**Fig. 7:** Rietveld refinement of nominal  $\text{CsTlF}_3$  sample in  $\text{Fm-3m}$  space group with  $a = 9.5449(1)$  Å, with SPXD.

**Fig. 8:** (a) dc  $\chi$  (susceptibility) vs.  $T$  of  $\text{CsTlCl}_3\text{-t}$  (green),  $\text{CsTlCl}_3\text{-c}$  (red), and  $\text{CsTlF}_3$  (blue) measured at field  $H = 1$  T. (b) Magnetic isotherms collected at  $T = 1.8$  K, colors as in (a). The solid lines correspond to the superposition of a Brillouin function with a linear component.

**Fig. 9:** (a)  $\text{Tl-L}_3$  edges of  $\text{CsTlCl}_3\text{-t}$ ,  $\text{CsTlCl}_3\text{-c}$ , and  $\text{Tl}_2\text{O}_3$ ,  $\text{Cs}_2\text{TlCl}_5$  and  $\text{TlCl}$  standards. (b) An expanded view of the  $\text{Tl-L}_3$  pre-edges. The 6s-hole related feature of  $\text{CsTlCl}_3\text{-c}$  (extracted by subtraction of a sp line fit background) is also shown on an enlarged vertical scale in the bottom of the figure.

**Fig. 10:**  $\text{Tl-L}_3$  edges of  $\text{CsTlF}_3$  along with those of  $\text{Tl}_2\text{O}_3$  and  $\text{TlF}$  standard. An expanded view of the  $\text{Tl-L}_3$  pre-edges is enlarged at the right bottom of the figure.

**Fig 11:** (a) Total density of states (DOS) and (b) optical conductivity of  $\text{CsTlCl}_3\text{-c}$ .

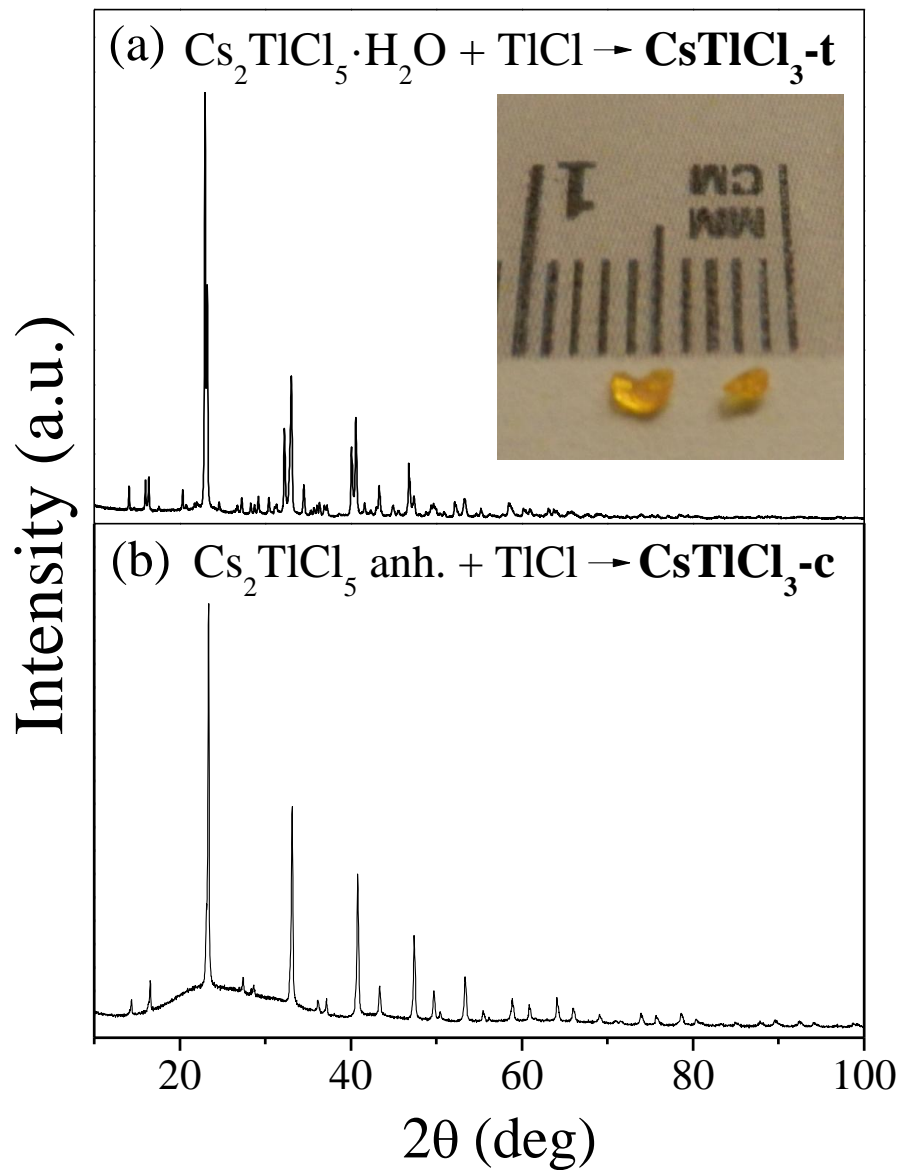


Fig. 1

M. Retuerto *et al.*

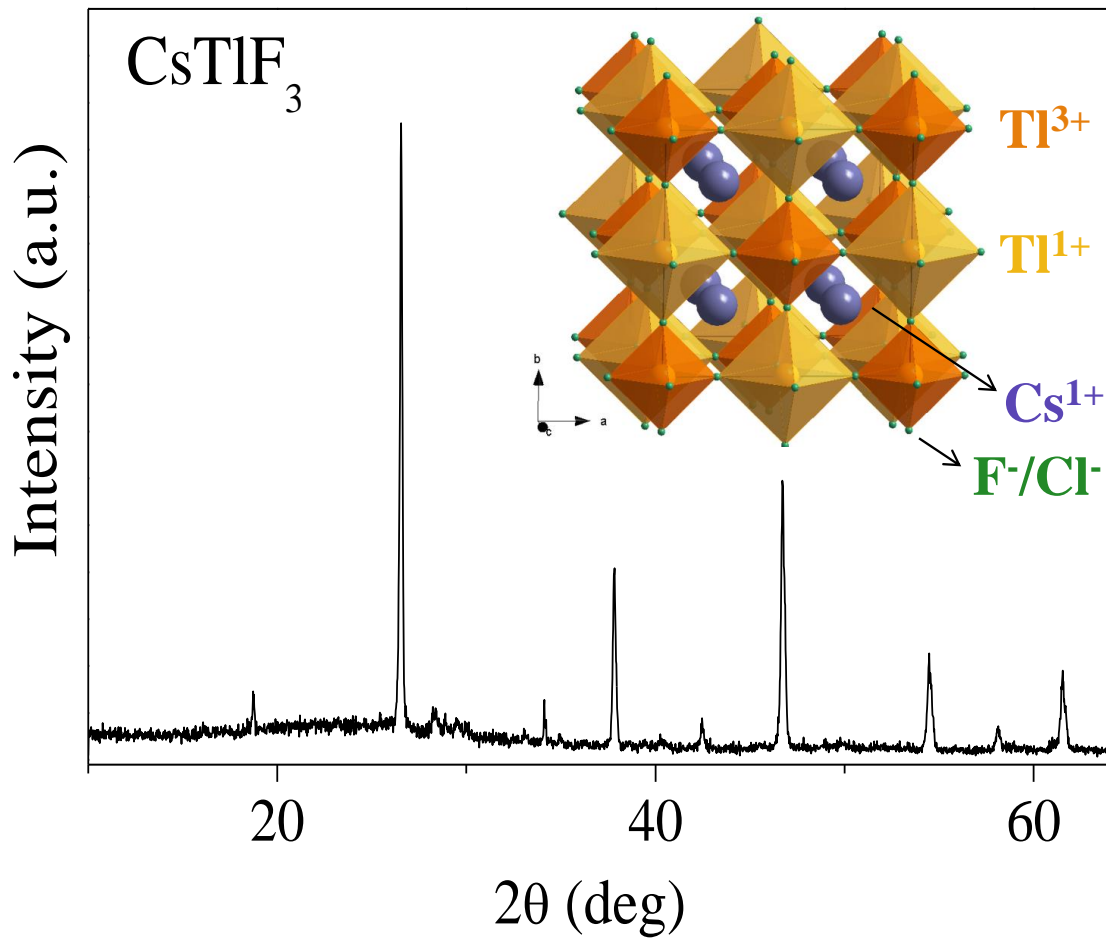


Fig. 2  
M. Retuerto *et al.*

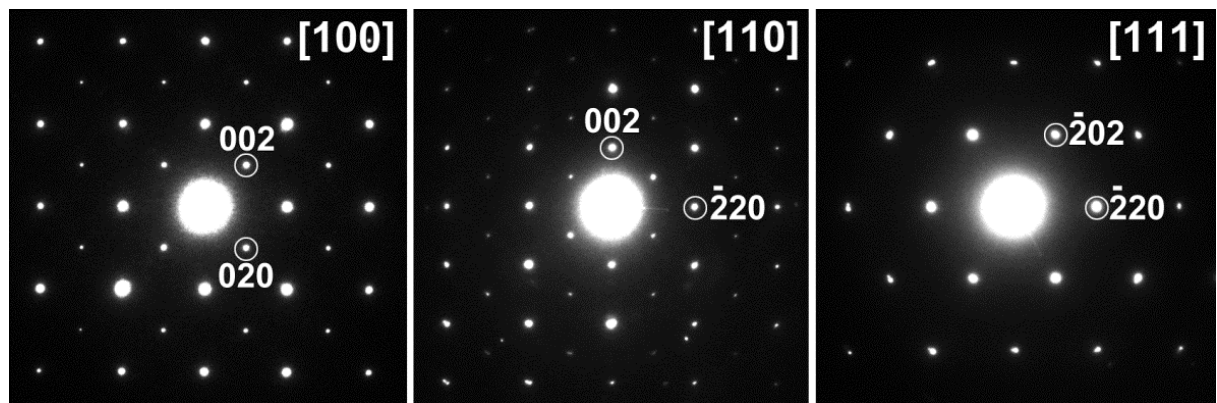


Fig. 3  
M. Retuerto *et al.*

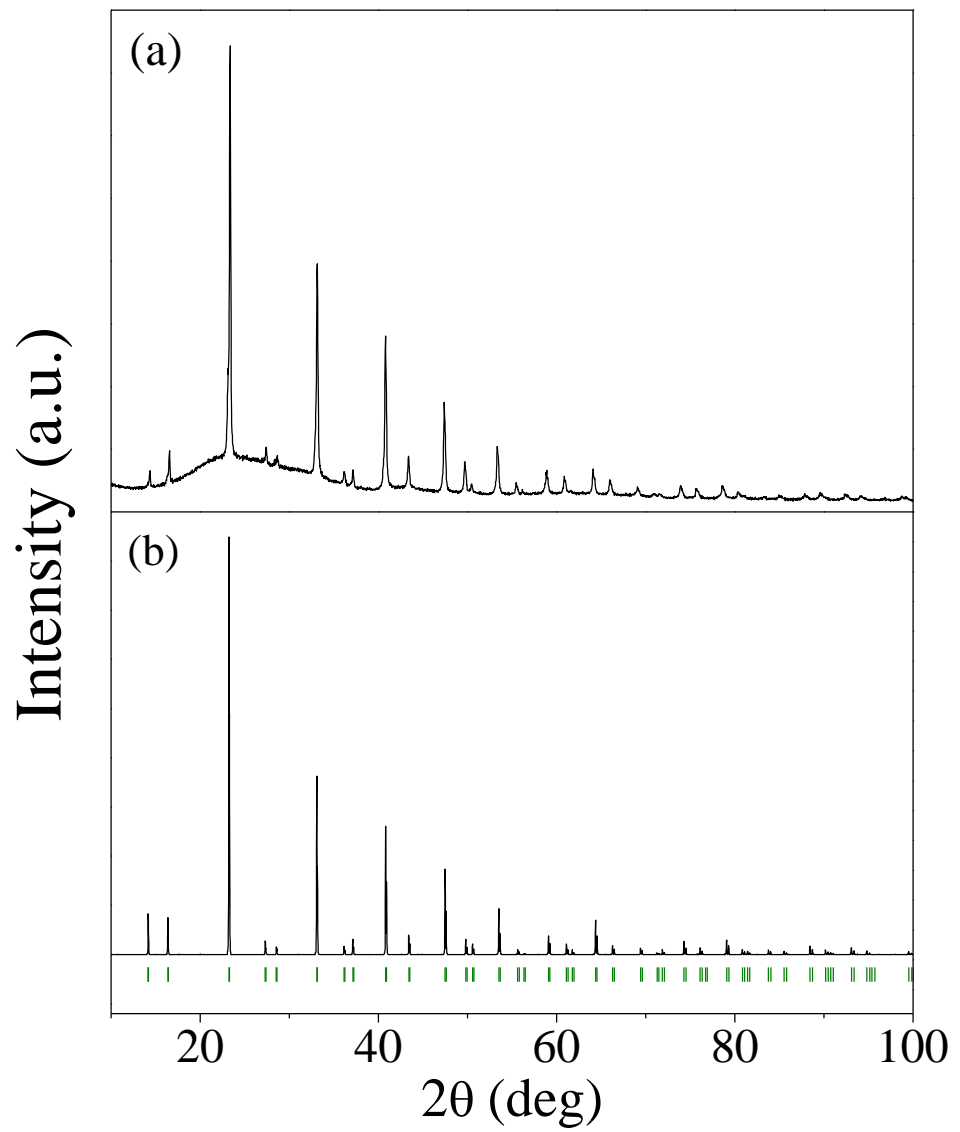


Fig. 4  
M. Retuerto *et al.*

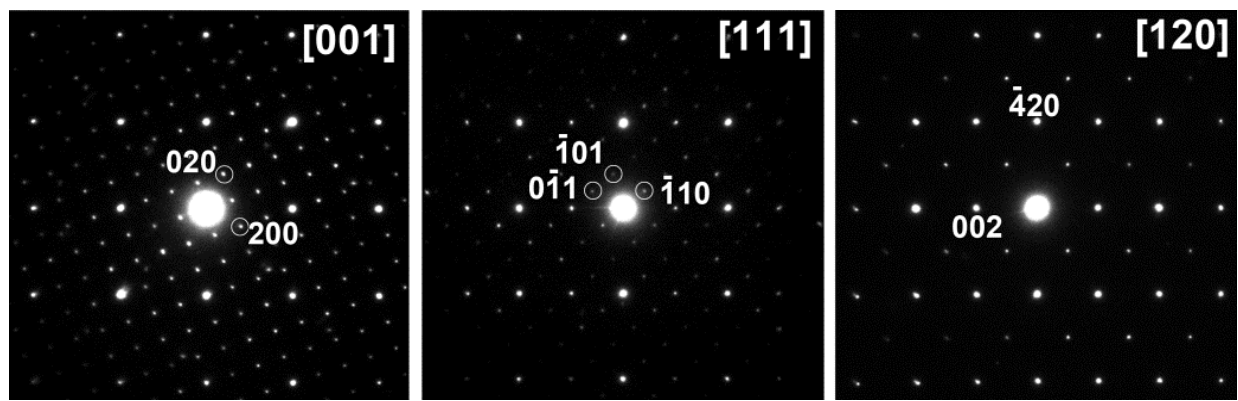


Fig. 5  
M. Retuerto *et al.*

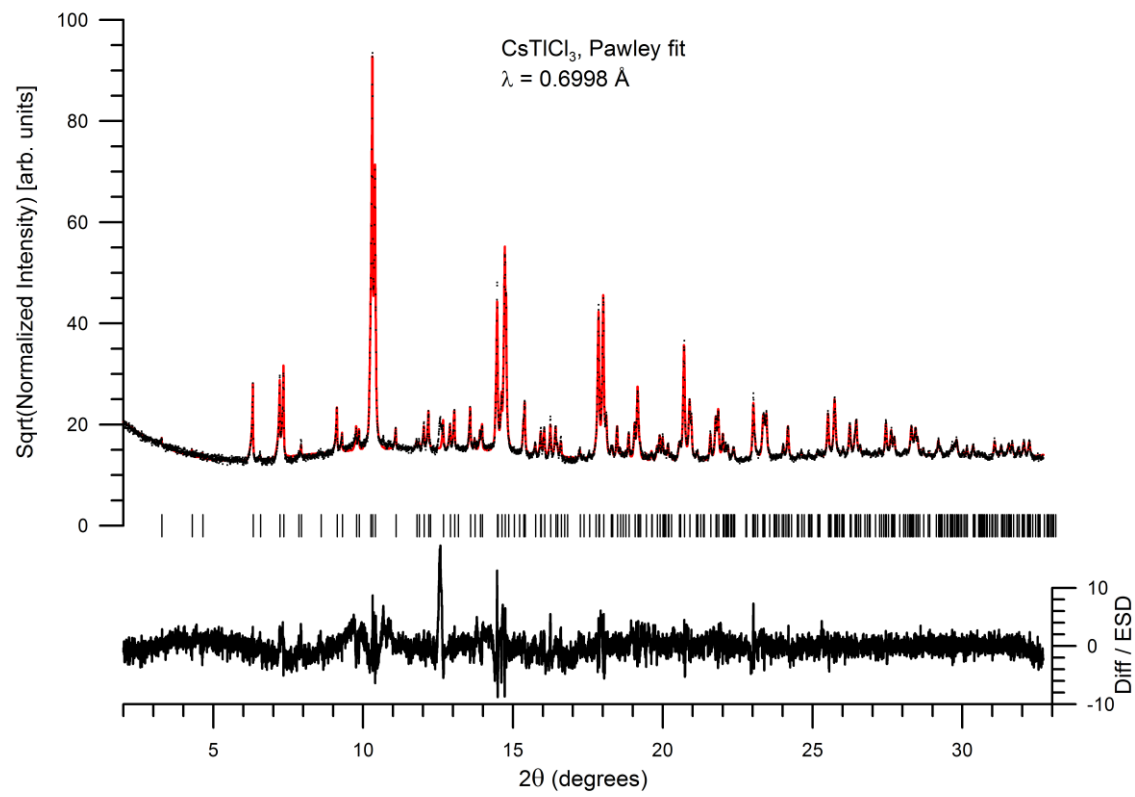


Fig. 6  
M. Retuerto *et al.*

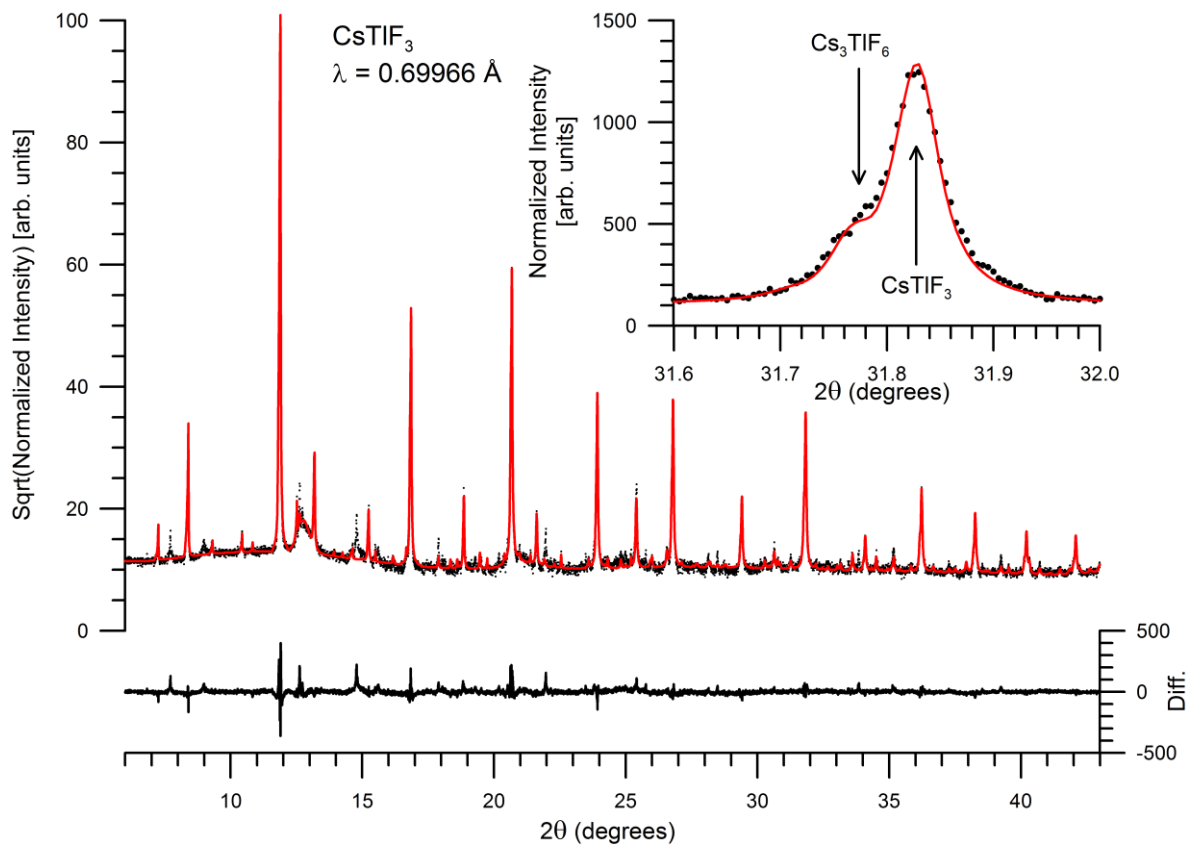


Fig. 7

M. Retuerto *et al.*

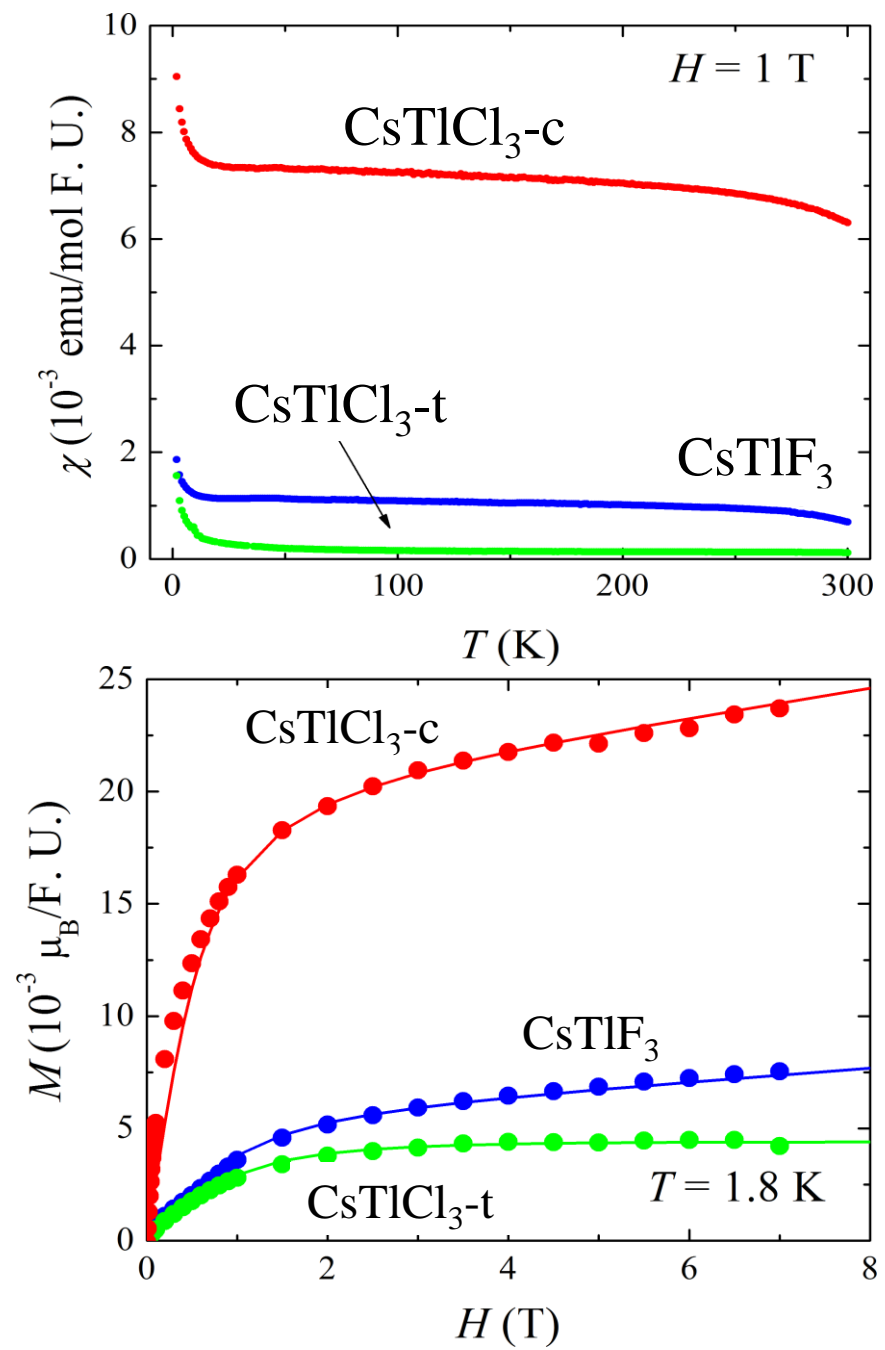


Fig. 8

M. Retuerto *et al.*

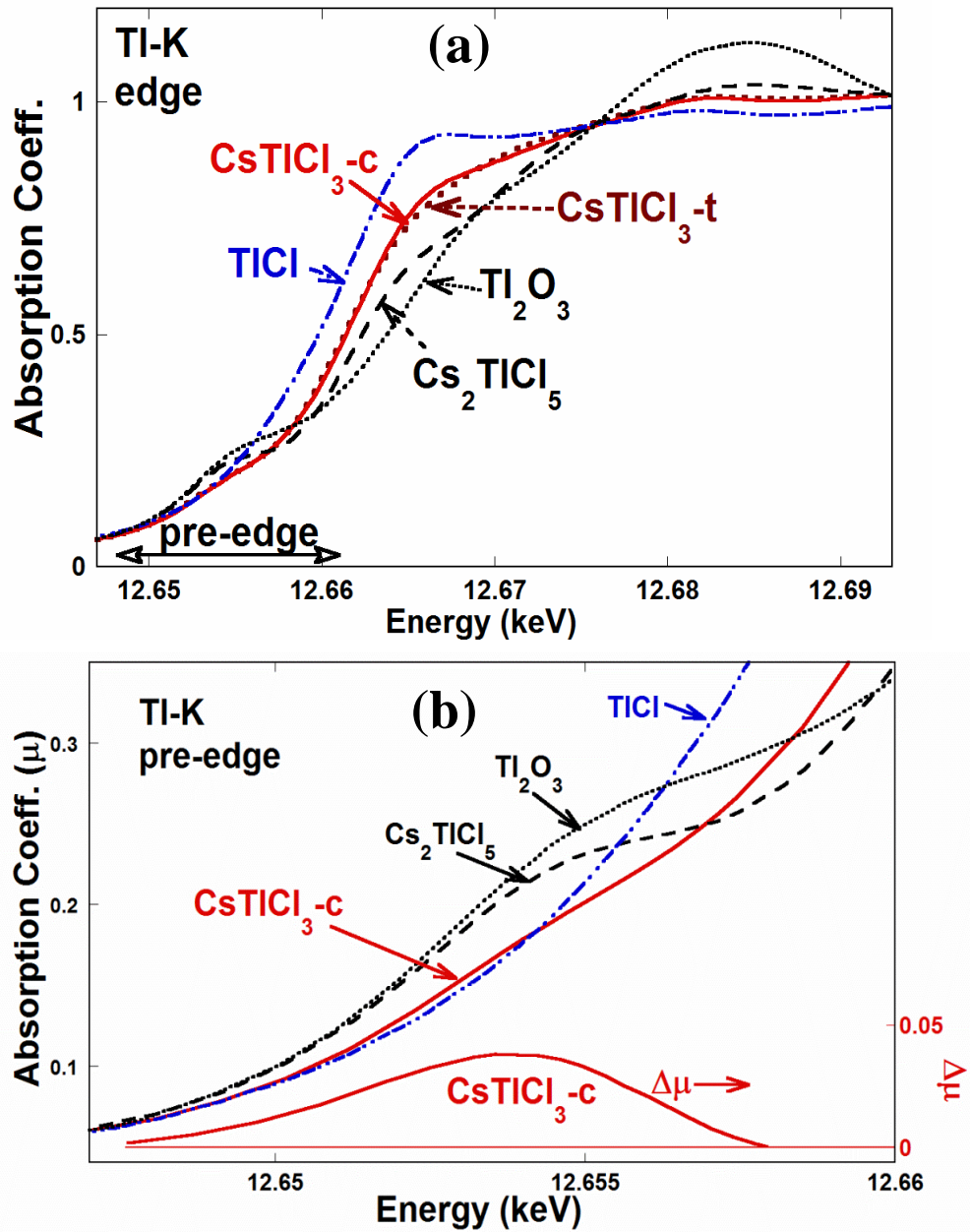


Fig. 9

M. Retuerto *et al.*

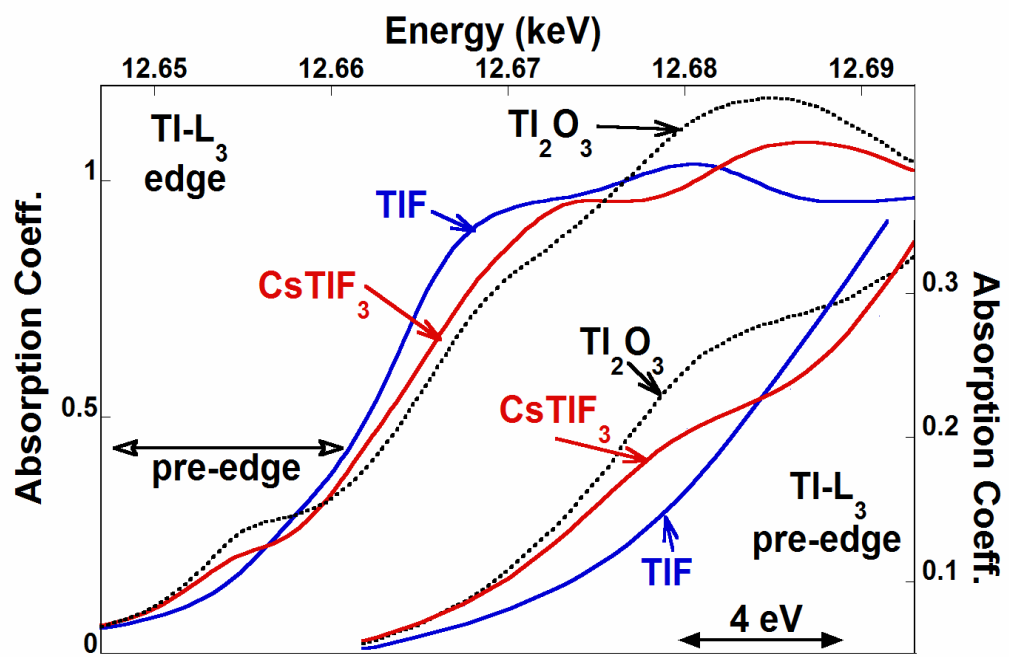


Fig. 10

M. Retuerto *et al.*

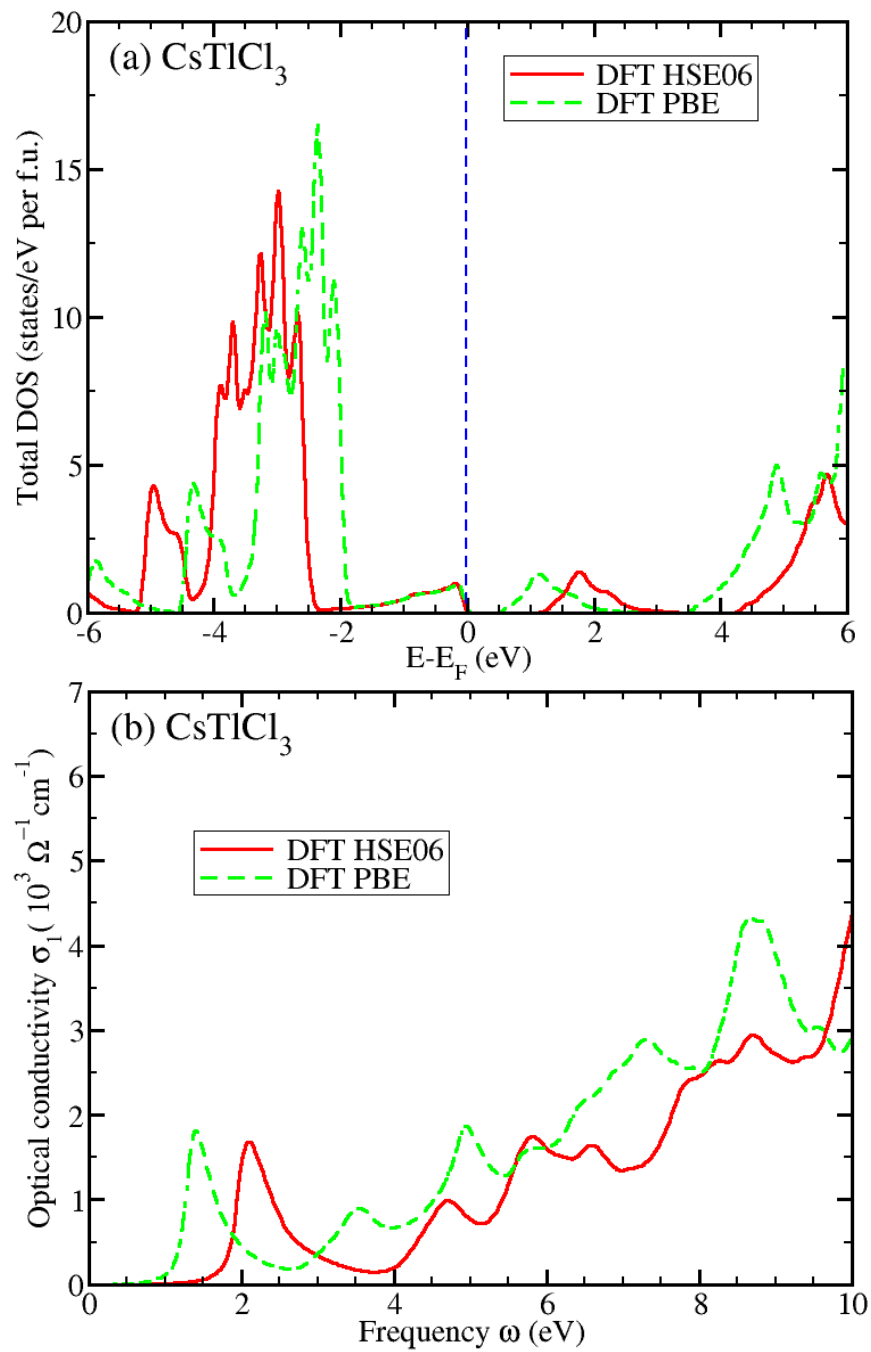


Fig. 11  
M. Retuerto *et al.*

## SUPPORTING INFORMATION

# Synthesis and properties of the theoretically predicted mixed-valent perovskite superconductors: $\text{CsTlX}_3$ ( $\text{X} = \text{F, Cl}$ )

M. Retuerto<sup>1</sup>, T. Emge<sup>1</sup>, M. R. Li<sup>1</sup>, Z. P. Yin<sup>2</sup>, M. C. Croft<sup>2</sup>, A. Ignatov<sup>2</sup>, J. W. Simonson<sup>3</sup>, M. C. Aronson<sup>3</sup>, P. W. Stephens<sup>4</sup>, J. Hadermann<sup>5</sup>, A. Pan<sup>6</sup>, D. N. Basov<sup>6</sup>, G. Kotliar<sup>2</sup>, M. Greenblatt<sup>1\*</sup>

<sup>1</sup> Department of Chemistry and Chemical Biology, Rutgers, The State University of New Jersey, 610 Taylor Road, Piscataway, NJ 08854, USA

<sup>2</sup> Department of Physics and Astronomy, Rutgers, The State University of New Jersey, 136 Frelinghuysen Road, Piscataway, NJ 08854, USA

<sup>3</sup> Brookhaven National Laboratory, Upton, NY 11973, USA

<sup>4</sup> Department of Physics & Astronomy State University of New York, Stony Brook, NY 11794, USA

<sup>5</sup> EMAT, Department of Physics, University of Antwerp, Groenenborgerlaan 171, 2020 Antwerp, Belgium

<sup>6</sup> Department of Physics, University of California San Diego, La Jolla, California 92093-0319, USA

**The supporting information is organized as follows:**

**1. Experimental Section**

- PXD of the precursors:  $\text{Cs}_2\text{TlCl}_5 \text{ H}_2\text{O}$  (Fig. S1a) and  $\text{Cs}_2\text{TlCl}_5$  (Fig. S1b).
- PXD of  $\text{CsTlCl}_3\text{-t}$  using two different preparation methods.
- Thermal gravimetric analysis (TGA) and Differential Scanning Calorimetry (DSC) of  $\text{CsTlCl}_3\text{-t}$  in Ar gas from 25 to 800 °C.

**2. Single Crystal Structure Determination**

- Refinement results using mean atom positions and anharmonic ADP in program JANA2006
- Refinement results using split atom model and harmonic ADP in program SHELXL

**3. XAS Cl-K edge of  $\text{CsTlCl}_3\text{-t}$  and  $\text{CsTlCl}_3\text{-c}$ .**

**4. First-principles Calculations for  $\text{CsTlF}_3$ .**

## 1. Experimental Section

- PXD of the precursors:  $\text{Cs}_2\text{TlCl}_5 \text{ H}_2\text{O}$  (Fig. S1a) and  $\text{Cs}_2\text{TlCl}_5$  (Fig. S1b).

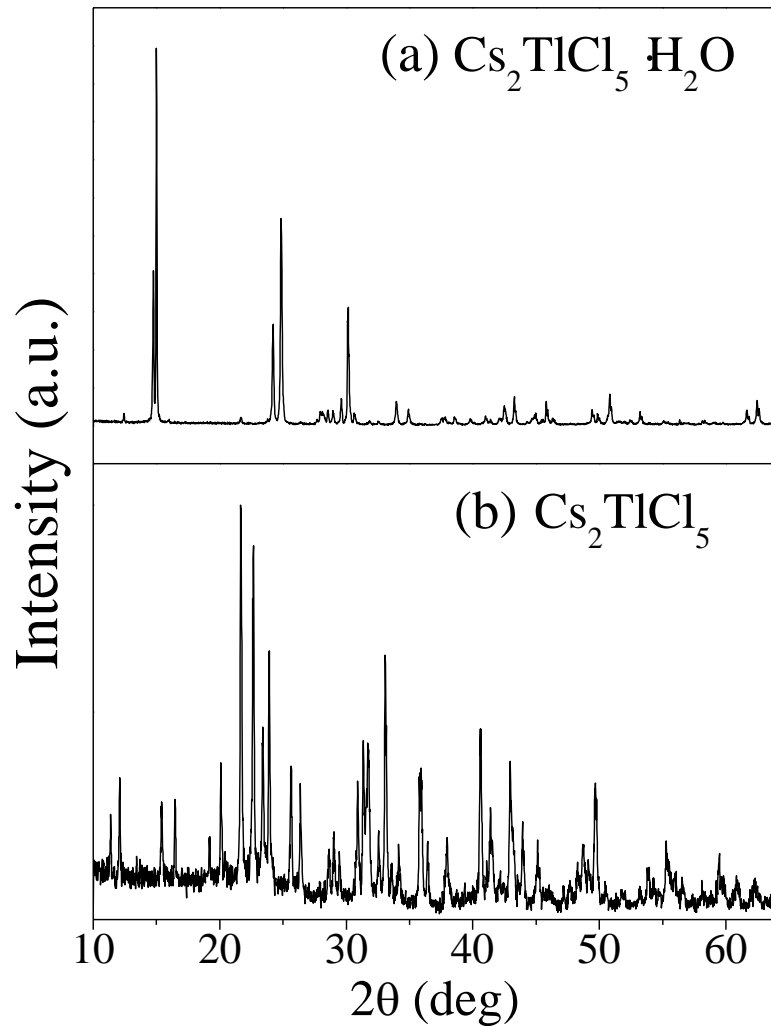


**Fig. S1:** PXD data of (a)  $\text{Cs}_2\text{TlCl}_5 \text{ H}_2\text{O}$  and (b)  $\text{Cs}_2\text{TlCl}_5$  precursors.

- PXD of  $\text{CsTlCl}_3\text{-t}$  synthesized using two different preparation methods: Fig. S2a: using  $\text{Cs}_2\text{TlCl}_5 \text{H}_2\text{O} + \text{TlCl}$  as starting materials. Fig. S2b using  $\text{TlCl}$ ,  $\text{CsCl}$  and  $\text{TlCl}_3 \text{xH}_2\text{O}$  as starting materials.

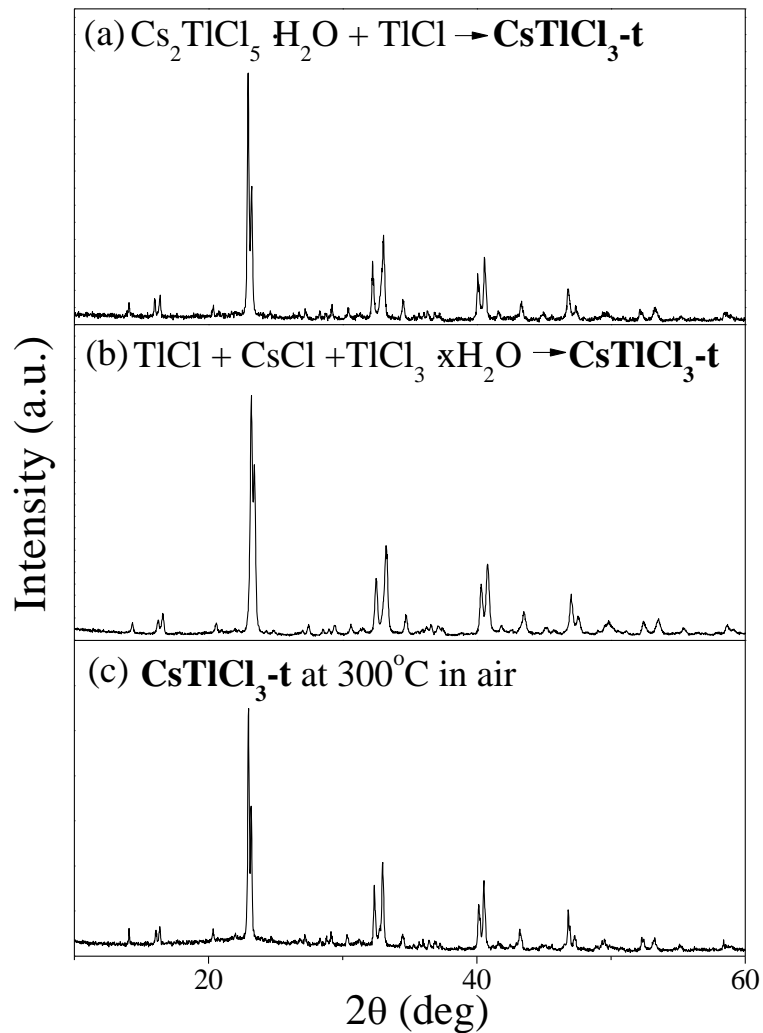


**Fig. S2:** PXD patterns of  $\text{CsTlCl}_3\text{-t}$  (a)(b) synthesized using two different preparation methods and (c) heated at  $300^\circ\text{C}$  in air.

- A thermal gravimetric analysis (TGA) coupled with a Differential Scanning Calorimetry (DSC) of  $\text{CsTlCl}_3\text{-t}$  was performed in Ar gas from 25 to 800 °C, in a SDT Q600 system, in order to analyze the evolution of  $\text{CsTlCl}_3$  in an open system, evaluate the quantity of water and a possible phase transition. As shown in Fig. 5, the compound is stable upto ~350-400 °C where the melting of the phase occurs; above ~350 °C the mass starts decreasing until complete evaporation of the sample around ~800 °C. Up to ~350 °C the tetragonal  $\text{CsTlCl}_3\text{-t}$  phase is stable without any phase transition observed.

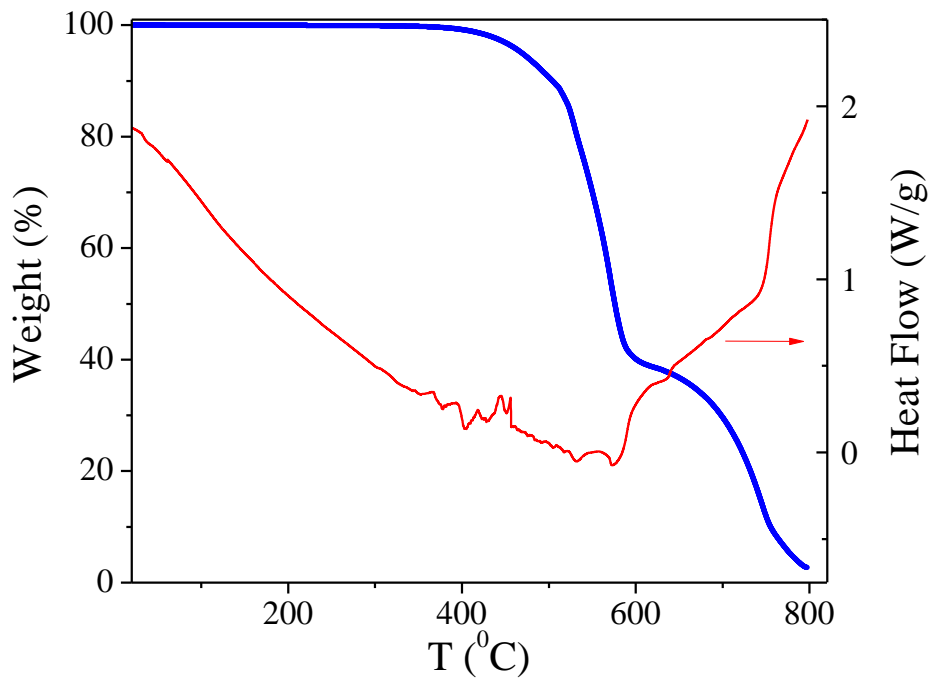


**Fig. S3:** TGA and DSC of  $\text{CsTlCl}_3\text{-t}$  in Ar gas from 25 to 800 °C.

## 2. Single Crystal Structure Determination

### Refinement results using mean atom positions and anharmonic ADP in program JANA2006

Table S2.1.1. Crystal data and structure refinement for  $\text{CsTlCl}_3\text{-c}$ , using the anharmonic ADP model (JANA2006)

Identification code	$\text{CsTlCl}_3\text{-c}$
Empirical formula	$\text{Cl}_6 \text{Cs}_2 \text{Tl}_1\text{.4}$
Formula weight	812.2
Temperature	100(2) K
Wavelength	0.71073 Å
Crystal system	Cubic
Space group	$\text{Fm-3}m$
Unit cell dimensions	$a = 10.8226(14)$ Å
Volume	1267.6(3) Å <sup>3</sup>
Z	4
Density (calculated)	4.31 Mg/m <sup>3</sup>
Absorption coefficient	30.7 mm <sup>-1</sup>
F(000)	1391
Weighting	$w = 1/(\sigma^2(F) + 0.01F^2)$
Crystal size	0.09 x 0.07 x 0.04 mm <sup>3</sup>
Theta range for data collection	5.33 to 32.52 °
Index ranges	-16 <= h <= 16, -15 <= k <= 16, -15 <= l <= 16
Reflections collected	4189
Independent/used reflections	155 [R(int) = 0.036] / 152
Completeness to theta = 32.52 °	98.1 %
Max. and min. transmission	0.384 and 0.176
Refinement method	Full-matrix least-squares on $F^2$
Isotropic extinction coefficient	0.0190
Data / restraints / parameters	152 / 2 / 25
Goodness-of-fit on $F^2$	1.4
Final R indices [ $I > 2\sigma(I)$ ]	$R_1 = 0.068, wR_2 = 0.128$
R indices (all data)	$R_1 = 0.070, wR_2 = 0.134$
Largest diff. peak and hole	6.5 and -3.1 e.Å <sup>-3</sup>

## Refinement results using split atom model and harmonic ADP in program SHELXL

Table S2.2.1. Crystal data and structure refinement for  $\text{CsTlCl}_3\text{-c}$ , using the split atom model (SHELXL).

Identification code	$\text{CsTlCl}_3\text{-c}$
Empirical formula	$\text{Cl}_6 \text{Cs}_2 \text{Tl}_1.79$
Formula weight	843.83
Temperature	100(2) K
Wavelength	0.71073 Å
Crystal system	Cubic
Space group	$\text{Fm-3}m$
Unit cell dimensions	$a = 10.8226(14)$ Å Volume $1267.6(3)$ Å $^3$
Z	4
Density (calculated)	4.42 Mg/m $^3$
Absorption coefficient	29.6 mm $^{-1}$
F(000)	1427
Crystal size	0.09 x 0.07 x 0.04 mm $^3$
Theta range for data collection	5.33 to 32.52 °
Index ranges	-16≤h≤16, -15≤k≤16, -15≤l≤16
Reflections collected	4167
Independent reflections	152 [R(int) = 0.038]
Completeness to theta = 32.52 °	98.1 %
Max. and min. transmission	0.384 and 0.176
Refinement method	Full-matrix least-squares on $F^2$
Data / restraints / parameters	152 / 101 / 29
Goodness-of-fit on $F^2$	1.02
Final R indices [I>2sigma(I)]	$R_1 = 0.023$ , $wR_2 = 0.054$
R indices (all data)	$R_1 = 0.023$ , $wR_2 = 0.054$
Largest diff. peak and hole	0.87 and -0.74 e.Å $^{-3}$

Table S2. Atomic coordinates and equivalent isotropic displacement parameters ( $\text{\AA}^2$ ) for  $\text{CsTlCl}_3\text{-c}$ , using the split atom model.  $U(\text{eq})$  is defined as one third of the trace of the orthogonalized  $U^{ij}$  tensor.

	x	y	z	$U(\text{eq})$
Tl(B)	0	0	0	0.024(1)
Cs1	0.2500	0.2500	0.2500	0.038(1)
Cs2	0.2791(10)	0.2209(10)	0.2209(10)	0.038(1)
Cs3	0.2500	0.2500	0.2059(12)	0.038(1)
Tl(B')1	0.5000	0	0	0.024(1)
Tl(B')2	0.4180(3)	0	0	0.024(1)
Tl(B')3	0.4414(12)	0	-0.586(12)	0.024(1)
Cl1	0.2373(2)	0	0	0.042(1)
Cl2	0	0.1682(8)	0.1682(8)	0.034(3)

Table S3. Anisotropic displacement parameters ( $\text{\AA}^2$ ) for  $\text{CsTlCl}_3\text{-c}$ . The anisotropic displacement factor exponent takes the form:  $-2\pi^2 [ h^2 a^{*2} U^{11} + \dots + 2 h k a^{*} b^{*} U^{12} ]$

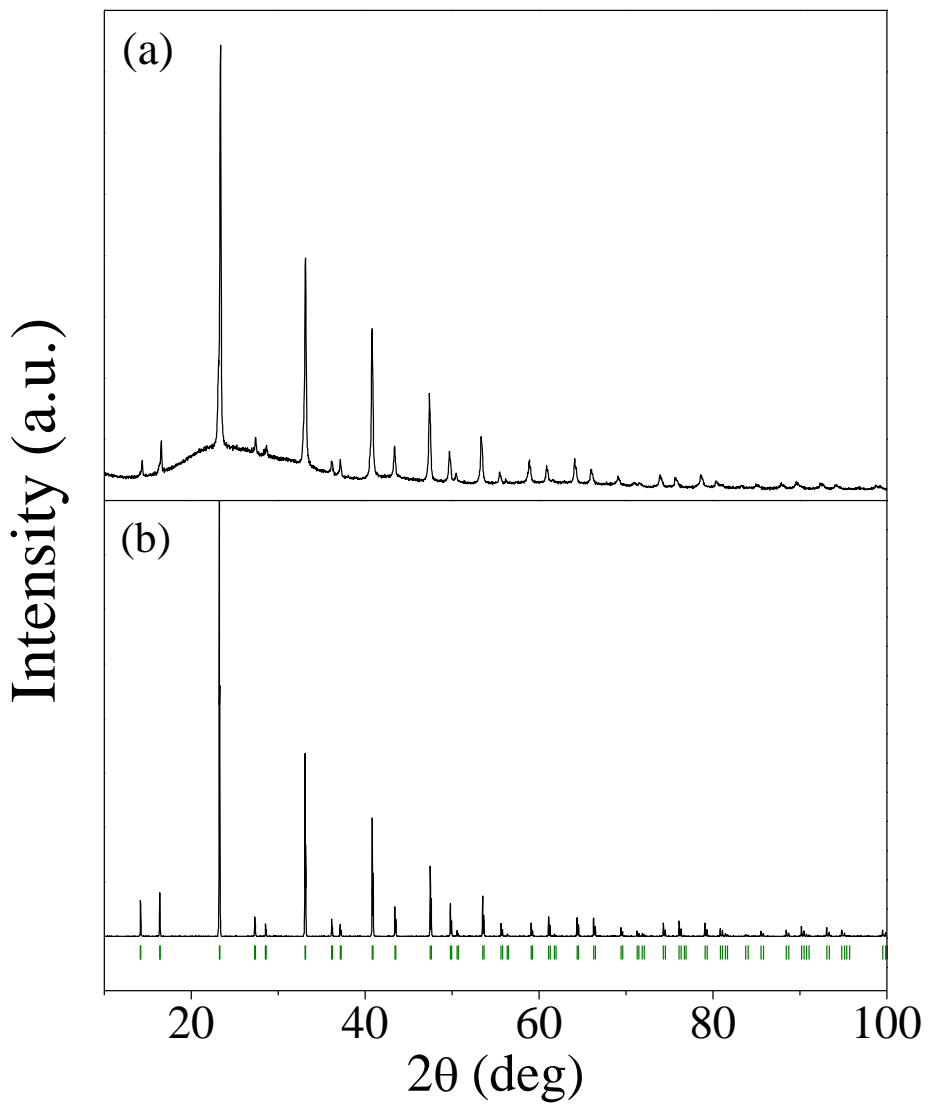
	U <sup>11</sup>	U <sup>22</sup>	U <sup>33</sup>	U <sup>23</sup>	U <sup>13</sup>	U <sup>12</sup>
Tl(B')1	0.038(2)	0.017(1)	0.017(1)	0.013(3)	-0.01(6)	0.02(8)
Tl(B')2	0.038(2)	0.017(1)	0.017(1)	0.013(3)	-0.01(6)	0.02(8)
Tl(B')3	0.038(2)	0.017(1)	0.017(1)	0.03(10)	-0.03(5)	0.01(10)
Cl1	0.028(1)	0.048(1)	0.048(1)	0	0	0
Cl2	0.033(5)	0.034(4)	0.034(4)	-0.013(5)	0	0

Table S4. Bond lengths [ $\text{\AA}$ ] for  $\text{CsTlCl}_3\text{-c}$ , using the split atom model.

Cs1-Cl1	12x3.8288(5)
Cs1-Cl2	1x2.981(5)
Cs1-Cl2	6x2.981(5)
Cs2-Cl1	6x 3.856(2), 3x3.412(14)
Cs2-Cl2	3x2.735(9), 3x3.126(7)
Cs2-Cl2	3x2.735(9), 3x3.464(18)
Cs3-Cl1	4x3.508(9), 2x3.8415(13), 2x3.875(2)
Cs3-Cl2	2x2.555(13), 4x3.156(9)
Cs3-Cl2	2x3.421(13), 4x2.876(4)
Tl(B)-Cl1	6x2.569(2)
Tl(B)-Cl2	6x2.575(13)
Tl(B)-Cl2	6x2.575(13)
Tl(B')1-Cl1	6x2.843(2)
Tl(B')2-Cl1	4x2.978(2), 1x1.955(4)
Tl(B')3-Cl1	2x2.297(9), 2x2.981(6)

Note: correlations with occupancies not taken into account.

---



**Fig. S4:** Comparison of (a) experimental PXD of  $\text{CsTlCl}_3\text{-c}$  and (b) Simulation from SCD using the split atom model.

### 3. XAS Cl-K edge of CsTlCl<sub>3</sub>-t and CsTlCl<sub>3</sub>-c.

The Cl-K near edge is dominated by dipole allowed 1s-to-2p transitions. The Cl-K near edges for a series of Cl compounds is shown in Fig S5. The simple structure less main-edge rise and broad peak for Cl<sup>-</sup> in NaCl and TlCl is typical for the ionic bonding and filled 2p orbitals in these materials. Cl<sup>5+</sup> in KClO<sub>3</sub>, on the other hand, displays an intense “white line” feature due to transitions into the now empty 2p orbitals, along with a very substantial chemical shift of the main edge to higher energy. The most striking structure in CsTlCl<sub>3</sub> spectra (Fig. S5) are the extremely intense pre-edge features (see the peak P in the figure) shifted well below the main edge rise. In transition metal compounds such Cl-K pre-edge features, associated with the metal d-orbital states hybridized with the ligand Cl-p states are common. Indeed the d-orbital sub-splitting, bandwidths, and energies have been studied with Cl-K XAS.<sup>1,2</sup> In the compounds considered here such pre-edge features are associated with transitions into Cl-2p states hybridized with Tl-6s hole states. For reference the Cl-K edge of the CsHgCl<sub>3</sub> perovskite standard, also shown, exhibits a similar prominent 6s-hole pre edge feature albeit shifted less far below the main edge. Here the larger shift of the Tl pre-edge feature reflects the lower energy of the Tl-6s relative to the Hg-6s states. The pre-edge of Tl<sup>3+</sup> in Cs<sub>2</sub>TlCl<sub>5</sub> manifests the pre-edge feature with the highest spectral intensity and the simplest/most-symmetrical structure. CsTlCl<sub>3</sub>-t and -c pre-edge feature are reproducibly shifted to lower energy and exhibit a lower spectral intensity in the main P-peak. Both spectra however evidence excess intensity and additional substructure between the P-peak and the main edge rise. See for examples the less deep minimum in intensity in the pre-edge region and the budge most prominently observed on the rising edge of CsTlCl<sub>3</sub>-t spectrum. Although detailed electronic structure calculations will be required to clarify these spectral features there is a definite disparity from pure Tl<sup>3+</sup> standard behavior. In the vicinity of the absorption coefficient value labelled E, Tl and Hg compounds are shifted to lower energy relative to TlCl and NaCl. This suggests that the hybridization of the metal 6s-states contributes some effective electron charge to the Cl. This observation also should be considered with electronic structure calculations.

1.Glaser, T.; Hedman, B.; Hodgson, K.; Solomon, E. I. *Acc. Chem. Res.* **2000**, *33*, 859-868. 2. Kozimor, S. A.; Yang, P.; Batista, E. R.; Boland, K. S.; Burns, C. J.; Clark, D. L.; Conradson, S. D.; Martin, R. L.; Wilkerson, M. P.; Wolfsberg, L. *E. J. Am. Chem. Soc.* **2009**, *131*, 12125-12136.

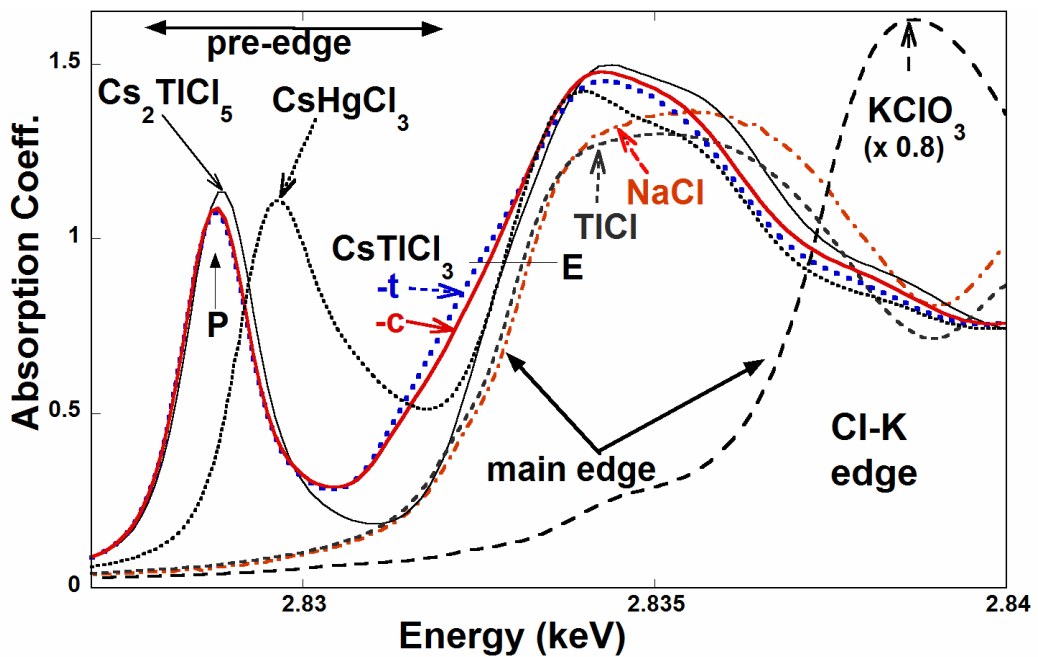


**Fig. S5:** The Cl-K edges of  $\text{CsTiCl}_3$ -t and -c, along with a number of standards. Note the  $\text{KClO}_3$  spectrum has been multiplied by a factor of 0.8 to facilitate comparison on a similar vertical scale. The prominent pre edge feature of the  $\text{CsTiCl}_3$  compounds has been labeled “P” and an absorption coefficient at which to compare the energy of the main edge rise has been labeled “E”.

#### 4. First-principles Calculations for CsTlF<sub>3</sub>:

We have also carried out first-principles density functional theory calculations with the VASP code<sup>1</sup> for the cubic CsTlF<sub>3</sub> with the experimentally determined lattice constants ( $a=9.5449$  angstrom) and atomic positions (F at (0.223, 0, 0)) in the Fm-3m space group. In addition to a generalized gradient approximation<sup>2</sup> (GGA [PBE version]) exchange-correlation functional, a *screened* hybrid functional HSE06<sup>3</sup> has been adopted to account for the non-local correlation in this compound. The corresponding total density of states (DOS) and optical conductivity of CsTlF<sub>3</sub> is presented in Fig. S6. The indirect band gap and the optical gap are estimated by DFT-HSE06 to be about 3.9 eV and 4.6 eV, respectively. Compared to DFT-HSE06, DFT-PBE underestimates the indirect band gap and optical gap by 1.2 eV, similar to the case of CsTlCl<sub>3</sub>.

With the experimental lattice constant  $a=9.5449$  angstrom, we have also relaxed the F position ( $x, 0, 0$ ) in the Fm-3m space group using DFT-HSE06 and DFT-PBE, and obtained optimized values of  $x \sim 0.226$  and 0.230, respectively. Again, the DFT-HSE06 optimized value agrees better with the experimental value of  $x=0.223(1)$ , while DFT-PBE substantially underestimates the F breathing distortion.

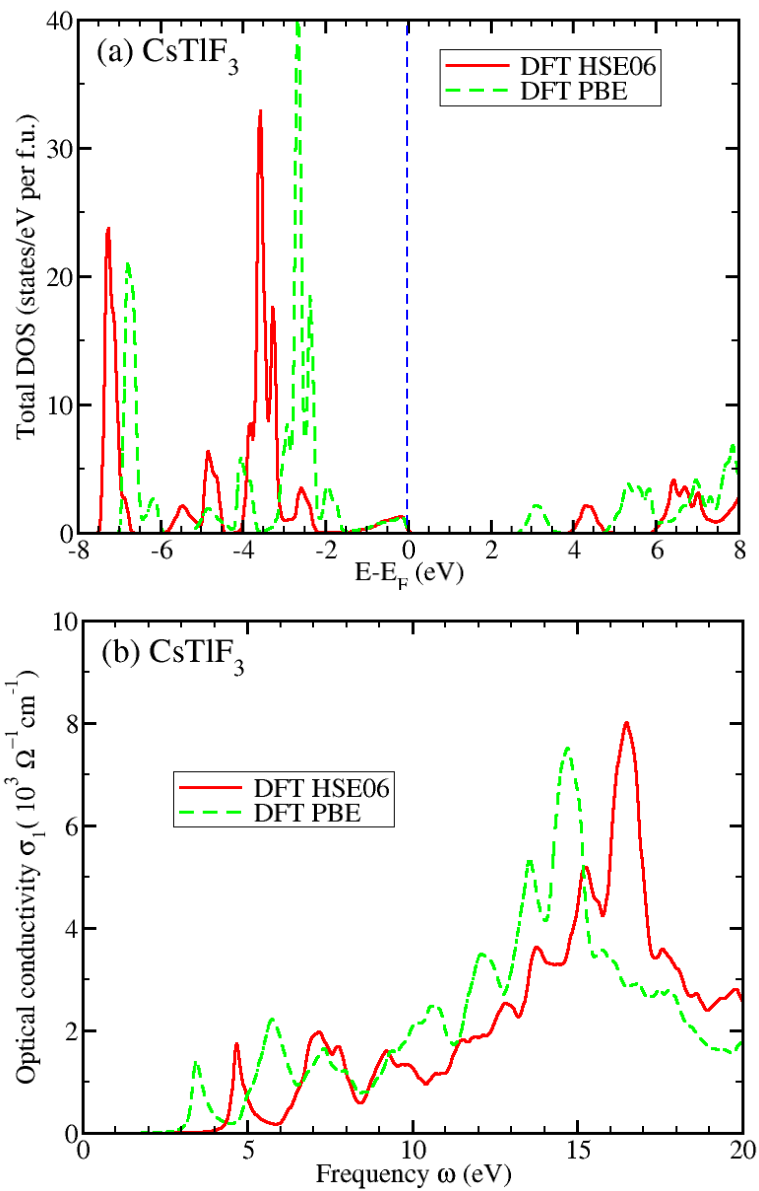


**Fig S6:** (a) Total density of states (DOS) and (b) optical conductivity of  $\text{CsTlF}_3$ .

1. Kresse G.; Furthmuller, J. *Comput. Mat. Sci.* **1996**, *6*, 15-50.
2. Perdew, J. P.; Burke, K.; Ernzerhof, M. *Phys. Rev. Lett.* **1996**, *77*, 3865-3868.
3. Krukau, A. V.; Vydrov, O. A.; Izmaylov, A. F.; Scuseria, G. E. *J. Chem. Phys.* **2006**, *125*, 224106.